AD-A058 982 AIR FORCE GEOPHYSICS LAB HANSCOM AFB MASS F/G 4/1
VARIABILITY OF THE LOWER THERMOSPHERE DETERMINED FROM SATELLITE--ETC(U)
MAY 78 F A MARCOS, R E MCINERNEY

UNCLASSIFIED AFGL-TR-78-0134 NL

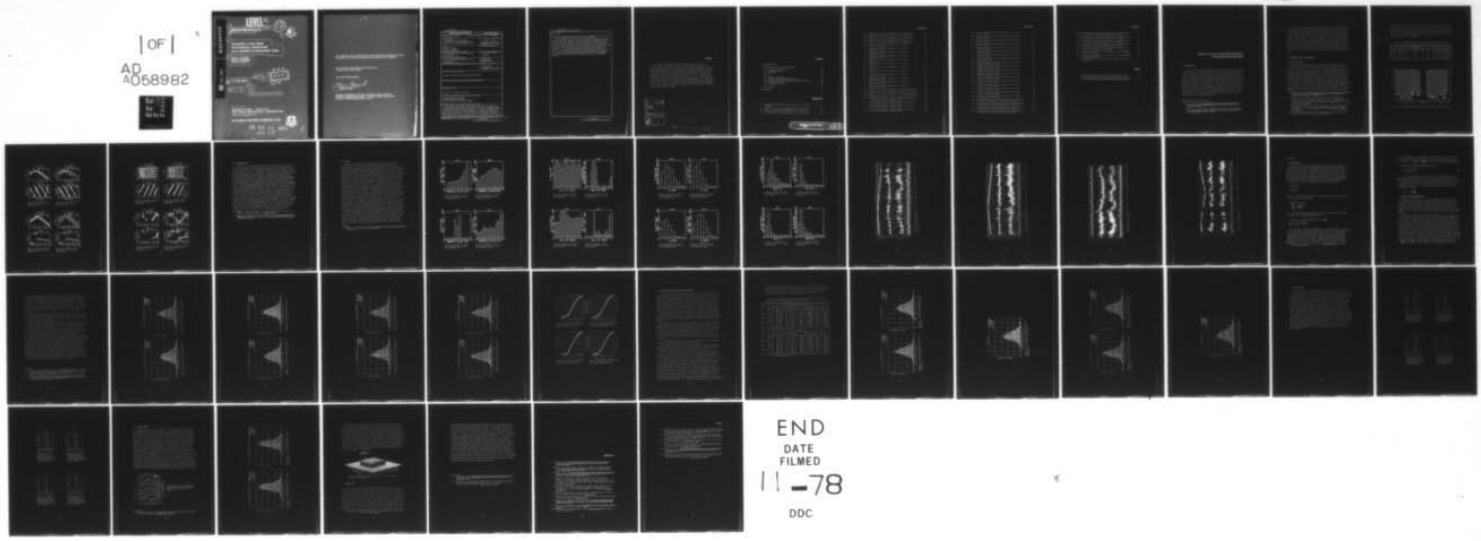

END
DATE FILMED
11-78
DDC

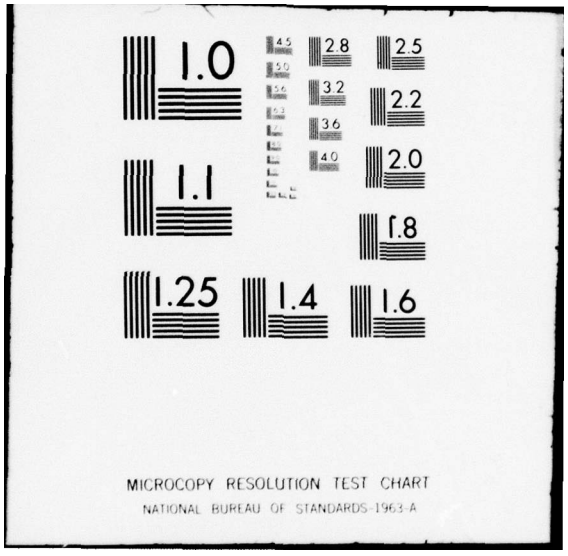
1.0
1.1
1.25
1.4
1.6
2.8
2.5
3.2
2.2
3.6
2.0
4.0
1.8
MICROCOPY RESOLUTION TEST CHART
NATIONAL BUREAU OF STANDARDS-1963-A

AD A058982

DDC FILE COPY

LEVEL II

(14) AFGL-TR-78-0134, AFCL-ERP-633
(9) ENVIRONMENTAL RESEARCH PAPERS, NO. 633

(12)

(6)

Variability of the Lower Thermosphere Determined from Satellite Accelerometer Data

(10) FRANK A. MARCOS,
ROBERT E. McINERNEY
ROBERT W. FIORETTI

DDC
RECEIVED
SEP 22 1978
E

(12) 46p.

(11) 25 May 1978

(26) 6690 (17) 04

Approved for public release; distribution unlimited.

62101F

AERONOMY DIVISION PROJECT 6690
AIR FORCE GEOPHYSICS LABORATORY
HANSCOM AFB, MASSACHUSETTS 01731

AIR FORCE SYSTEMS COMMAND, USAF

78 09 21 005
409 578

This report has been reviewed by the ESD Information Office (OI) and is releasable to the National Technical Information Service (NTIS).

This technical report has been reviewed and is approved for publication.

FOR THE COMMANDER

John Howard

Chief Scientist

Qualified requestors may obtain additional copies from the Defense Documentation Center. All others should apply to the National Technical Information Service.

Unclassified

SECURITY CLASSIFICATION OF THIS PAGE (When Data Entered)

REPORT DOCUMENTATION PAGE		READ INSTRUCTIONS BEFORE COMPLETING FORM
1. REPORT NUMBER AFGL-TR-78-0134	2. GOVT ACCESSION NO.	3. RECIPIENT'S CATALOG NUMBER
4. TITLE (and Subtitle) VARIABILITY OF THE LOWER THERMOSPHERE DETERMINED FROM SATELLITE ACCELEROMETER DATA		5. TYPE OF REPORT & PERIOD COVERED Scientific. Interim. 6. PERFORMING ORG. REPORT NUMBER ERP No. 633
7. AUTHOR(s) Frank A. Marcos Robert E. McInerney Robert W. Fioretti*		8. CONTRACT OR GRANT NUMBER(s)
9. PERFORMING ORGANIZATION NAME AND ADDRESS Air Force Geophysics Laboratory (LKB) Hanscom AFB Massachusetts 01731		10. PROGRAM ELEMENT, PROJECT, TASK AREA & WORK UNIT NUMBERS 66900403
11. CONTROLLING OFFICE NAME AND ADDRESS Air Force Geophysics Laboratory (LKB) Hanscom AFB Massachusetts 01731		12. REPORT DATE 25 May 1978 13. NUMBER OF PAGES 46
14. MONITORING AGENCY NAME & ADDRESS(if different from Controlling Office)		15. SECURITY CLASS. (of this report) Unclassified 15a. DECLASSIFICATION/DOWNGRADING SCHEDULE

16. DISTRIBUTION STATEMENT (of this Report)

Approved for public release; distribution unlimited.

17. DISTRIBUTION STATEMENT (of the abstract entered in Block 20, if different from Report)

18. SUPPLEMENTARY NOTES

*RDP, Inc., Waltham, MA 02154

19. KEY WORDS (Continue on reverse side if necessary and identify by block number)

Satellite accelerometer data
Neutral density measurements
Lower thermospheric density variability

20. ABSTRACT (Continue on reverse side if necessary and identify by block number)

An extensive atmospheric density data base has been developed using accelerometer results from four low altitude satellites. The data were obtained with the NASA Atmosphere Explorer -C, -D, and -E satellites and the Air Force S3-1 satellite. Measurements were made on over 4000 orbits during the period January 1974 to November 1976. The altitude range of the data is from 250 km down to as low as 140 km, with latitude coverage from 90°N to 90°S and local time periods that cover several 24-hr cycles. The data were obtained over a wide range of geomagnetic activity conditions. Solar

→ next page

DD FORM 1 JAN 73 1473 EDITION OF 1 NOV 65 IS OBSOLETE

Unclassified

SECURITY CLASSIFICATION OF THIS PAGE (When Data Entered)

20. (Contd)

radiation, as indicated by the 10.7-cm flux, was generally very low. Hence the data base applies mainly to solar minimum conditions.

A description of the satellites, the accelerometer experiment, and the data base is given. Density variability is statistically analyzed in relation to selected atmospheric models. Particular attention is given to deviations from a normal distribution. Frequency distributions of the data are described in terms of the mean value and the second, third, and fourth moments about the mean. This provides a more accurate description of extreme variations. The statistical properties of atmospheric variability are analyzed as a function of geomagnetic activity, latitude, altitude, and local time to develop a quantitative knowledge of unmodeled density variations. The results show that these accelerometer data will permit significant improvement in understanding the variations in the lower thermospheric density.

Preface

The authors are indebted to Shirley Cieszka, Lawrence Cox, and Dr. C. John McCann, RDP, Inc., who were involved in various aspects of the Atmosphere Explorer satellite data reduction, formation of the data base, development of plotting routines, and implementation of mathematical analyses. The S3-1 data reduction was carried out under AF Contract F19628-76-C-0190 with Boston College; Dennis Delorey was principal investigator. Dr. K.S.W. Champion was principal investigator for the accelerometer experiment on AE. John Kotelly, SUA, was contract manager for Contract F19628-73-C-0142 (with RDP, Inc.) under which the AE-C data were reduced. Ephemeris data were provided by Edward Robinson, SUA. The manuscript was reviewed by Edmund Murphy, LKD, and Dr. Felix Hoots, Office of Astrodynamics, ADCOM.

ACCESSION for
NTIS White Section X
DDC Buff Section ☐
UNANNOUNCED ☐
JUSTIFICATION
BY
DISTRIBUTION/AVAILABILITY CODES
Dist. AVAIL. and/or SPECIAL
A

78 09 21 005

Contents

1.	INTRODUCTION	9
2.	EXPERIMENT AND DATA DESCRIPTION	10
	2.1 Satellite Characteristics	10
	2.2 Drag Measurement	14
	2.3 Data Base	15
3.	RESULTS	24
	3.1 Statistical Properties	24
	3.2 Frequency and Probability Distributions	25
	3.3 Data as a Function of Geomagnetic Activity and Latitude	32
	3.4 Altitude Dependence	38
	3.5 Local Time Variations	41
4.	CONCLUSIONS	43
	REFERENCES	45

Illustrations

1.	Distribution of Density Data in an Altitude-Time Coordinate System	11
2a.	Latitude and Local Time Distribution for AE-C 160 km Data	12
2b.	Latitude and Local Time Distribution for AE-C 240 km Data	12
2c.	Latitude and Local Time Distribution for AE-D 160 km Data	12

PRECEDING PAGE NOT FILMED
BLANK

Illustrations

2d.	Latitude and Local Time Distribution for AE-D 240 km Data	12
2e.	Latitude and Local Time Distribution for AE-E 160 km Data	13
2f.	Latitude and Local Time Distribution for AE-E 240 km Data	13
2g.	Latitude and Local Time Distribution for S3-1 160 km Data	13
2h.	Latitude and Local Time Distribution for S3-1 240 km Data	13
3a.	Histogram of AE-C Data Distribution as a Function of Geographic Latitude	16
3b.	Histogram of AE-D Data Distribution as a Function of Geographic Latitude	16
3c.	Histogram of AE-E Data Distribution as a Function of Geographic Latitude	16
3d.	Histogram of S3-1 Data Distribution as a Function of Geographic Latitude	16
4a.	Histogram of AE-C Data Distribution as a Function of Local Time	17
4b.	Histogram of AE-D Data Distribution as a Function of Local Time	17
4c.	Histogram of AE-E Data Distribution as a Function of Local Time	17
4d.	Histogram of S3-1 Data Distribution as a Function of Local Time	17
5a.	Histogram of AE-C Data Distribution as a Function of Geomagnetic Activity	18
5b.	Histogram of AE-D Data Distribution as a Function of Geomagnetic Activity	18
5c.	Histogram of AE-E Data Distribution as a Function of Geomagnetic Activity	18
5d.	Histogram of S3-1 Data Distribution as a Function of Geomagnetic Activity	18
6a.	Histogram of AE-C Data Distribution as a Function of Solar Flux	19
6b.	Histogram of AE-D Data Distribution as a Function of Solar Flux	19
6c.	Histogram of AE-E Data Distribution as a Function of Solar Flux	19
6d.	Histogram of S3-1 Data Distribution as a Function of Solar Flux	19
7a.	AE-C Data Base at 180 km: Latitude, Density (g/cm^3) Ratio to J71 Model and K_p as a Function of Time	20
7b.	AE-D Data Base at 180 km: Latitude, Density (g/cm^3) Ratio to J71 Model and K_p as a Function of Time	21
7c.	AE-E Data Base at 180 km: Latitude, Density (g/cm^3) Ratio to J71 Model and K_p as a Function of Time	22
7d.	S3-1 Data Base at 180 km: Latitude, Density (g/cm^3) Ratio to J71 Model and K_p as a Function of Time	23

Illustrations

8a. Frequency Distribution of Percent Difference of AE-C Data from J71 Model 27

8b. Frequency Distribution of Percent Difference of AE-D Data from J71 Model 27

8c. Frequency Distribution of Percent Difference of AE-E Data from J71 Model 28

8d. Frequency Distribution of Percent Difference of S3-1 Data from J71 Model 28

9a. Frequency Distribution of Percent Difference of AE-C Data from MSIS Model 29

9b. Frequency Distribution of Percent Difference of AE-D Data from MSIS Model 29

9c. Frequency Distribution of Percent Difference of AE-E Data from MSIS Model 30

9d. Frequency Distribution of Percent Difference of S3-1 Data from MSIS Model 30

10a. Probability Distributions for AE-C Data Shown as Percent Departure from the J71 Model 31

10b. Probability Distributions for AE-D Data Shown as Percent Departure from the J71 Model 31

10c. Probability Distributions for AE-E Data Shown as Percent Departure from the J71 Model 31

10d. Probability Distributions for S3-1 Data Shown as Percent Departure from the J71 Model 31

11a. Frequency Distribution of Percent Difference of S3-1 Data for $K_p < 3_-$ from J71 Model 34

11b. Frequency Distribution of Percent Difference of S3-1 Data for $K_p \geq 4_o$ from J71 Model 34

11c. Frequency Distribution of Percent Difference of S3-1 Data for $K_p \geq 5_o$ from J71 Model 35

12a. Frequency Distribution of Percent Difference of S3-1 Data for $K_p < 3_-$ from J71 Model 36

12b. Frequency Distribution of Percent Difference of S3-1 Data for $K_p \geq 4_o$ from MSIS Model 36

12c. Frequency Distribution of Percent Difference of S3-1 Data for $K_p \geq 5_o$ from MSIS Model 37

13a. Percent Deviation from the J71 Model of the Mean and Standard Deviations of AE-C Density Measurements vs Altitude 39

13b. Percent Deviation from the J71 Model of the Mean and Standard Deviations of AE-D Density Measurements vs Altitude 39

13c. Percent Deviation from the J71 Model of the Mean and Standard Deviations of AE-E Density Measurements vs Altitude 39

13d. Percent Deviation from the J71 Model of the Mean and Standard Deviations of S3-1 Density Measurements vs Altitude 39

Illustrations

14a. Percent Deviation from the MSIS Model of the Mean and Standard Deviations of AE-C Density Measurements vs Altitude 40

14b. Percent Deviation from the MSIS Model of the Mean and Standard Deviations of AE-D Density Measurements vs Altitude 40

14c. Percent Deviation from the MSIS Model of the Mean and Standard Deviations of AE-E Density Measurements vs Altitude 40

14d. Percent Deviations from the MSIS Model of the Mean and Standard Deviations of S3-1 Density Measurements vs Altitude 40

15. Local Time Variation of AE-E Density Data at 160, 200, and 240 km; Ratio of Data to J71 and MSIS 41

16a. Frequency Distributions of Percent Difference of AE-E 0800-0900 Data from J71 Model 42

16b. Frequency Distributions of Percent Difference of AE-E 0800-0900 Data from MSIS Model 42

17. Altitude Dependence of AE-E Local Time Variations (Normalized to 200 km) 43

Tables

1. Satellite Orbital Characteristics and Data Acquisition Periods 11

2. Mean and Standard Deviation as Percent Deviation from J71 and MSIS Models for S3-1 Low and High K_p Data Group vs Latitude 33

Variability of the Lower Thermosphere Determined From Satellite Accelerometer Data

1. INTRODUCTION

Accurate density measurements have been previously made with electrostatic accelerometers on low altitude satellites.[1,2] These in situ data permitted detailed analysis of atmospheric behavior compared to the orbital decay technique which involves considerable temporal and spatial averaging. Because these satellite lifetimes were relatively short, however, only limited amounts of the accelerometer data were available. This report describes an extensive neutral density data base generated using data from accelerometers on four low altitude satellites (Atmosphere Explorer -C, -D, and -E, hereafter AE-C, -D, and E, and Air Force satellite S3-1). Data obtained from over 4000 orbits (a total of 115,951 discrete values) at altitudes from 250 km down to as low as 140 km during the period January 1974 to November 1976, have been utilized. This represents the most extensive set of neutral density measurements in existence.

(Received for publication 25 May 1978)

1. Devries, L. L. (1971) Experimental Evidence in Support of Joule Heating Associated With Geomagnetic Activity, Marshall Space Flight Center, NASA TM X-64568.

2. Marcos, F. A., McInerney, R., Corbin, J., Fioretti, R., and Grossbard, N. (1972) Atmospheric Density Results Derived From the SPADES Satellite Accelerometer Data, AFCRL-72-0608.

Knowledge of atmospheric density and its variations is required for satisfactory low altitude satellite design, operation, and orbit prediction. Existing models of the lower thermosphere are deficient since they are primarily based on data obtained at higher altitudes. This report compares the accelerometer density values to two commonly used models, that of Jacchia[3] hereafter J71, and that of Hedin et al,[4,5] hereafter MSIS. Comparisons are made as a function of altitude, latitude, geomagnetic activity, and local time. Frequency distributions of these comparisons are described in terms of their mean value, standard deviation, coefficient of skewness and kurtosis. Results of this study provide a quantitative estimate of the improvements required in current models of the thermosphere. Correlations of the observed variations with solar and geophysical parameters will be described in forthcoming reports.

2. EXPERIMENT AND DATA DESCRIPTION

2.1 Satellite Characteristics

The Atmosphere Explorer program involved three low-altitude satellites designed to permit a coordinated study of the thermosphere. Dalgarno et al[6] have described the AE mission. AE-C, -D, and -E were launched into low-perigee high-eccentricity orbits with different inclinations. A propulsion system was used to maintain an elliptical orbit for approximately 1 year (AE-D data acquisitions were terminated after 3-1/2 months when the spacecraft power system failed. However, data were obtained on 81 percent of the orbits). AE-C and AE-E were put into circular orbits near 250 km following their elliptical orbit phase. Data in this report are for the elliptical orbit phase only. Data were acquired in both a spinning (4 rpm) and a despun mode. S3-1 was also launched into a low-perigee high-eccentricity orbit and was spin-stabilized at 5 rpm. This satellite had a lifetime of nearly seven months. Table 1 provides orbital characteristics and the dates of elliptical orbit

3. Jacchia, L.G. (1971) Revised Static Models of the Thermosphere and Exosphere With Empirical Temperature Profiles. Spec. Rept. 332, Smithsonian Astrophys. Observatory, Cambridge, MA.

4. Hedin, A.E., Salah, J.E., Evans, J.V., Reber, C.A., Newton, G.P., Spencer, N.W., Kayser, D.C., Alcayde, D., Bayer, P., Cogger, L., and McClure, J.P. (1977a) A global thermospheric model based on mass spectrometer and incoherent scatter data, MSIS 1, N_2 density and temperature. J. Geophys. Res. 82:2139.

5. Hedin, A.E., Reber, C.A., Newton, G.P., Spencer, N.W., Brinton, H.C., and Mayr, H.G. (1977b) A global thermospheric model based on mass spectrometer and incoherent scatter data, MSIS 2, Composition, J. Geophys. Res. 82:2148.

6. Dalgarno, A., Hanson, W.B., Spencer, N.W., and Schmerling, E.R. (1973) The Atmosphere Explorer mission, Radio Sci. 8:263.

data acquisition for each satellite. The altitudes at which data were obtained are shown (shaded areas) as a function of time in Figure 1. The AE-C and -E perigees were occasionally lowered to below 140 km. Perigee of S3-1 was generally between 160 and 180 km. Data obtained from 250 km down to 140 km are included in the data base. Figures 2a through 2h show the variation in latitude (top curve) and local time (bottom curve) for each satellite.

Table 1. Satellite Orbital Characteristics and Data Acquisition Periods

Satellite	Launch Data	End Elliptical Data Acquisition	Inclination	Initial Perigee	Initial Apogee
AE-C	Dec 73	Nov 74	68°	156 km	4000 km
S3-1	Oct 74	May 75	97°	160 km	4000 km
AE-D	Oct 75	Jan 76	90°	156 km	3800 km
AE-E	Nov 75	Nov 76	20°	157 km	3000 km

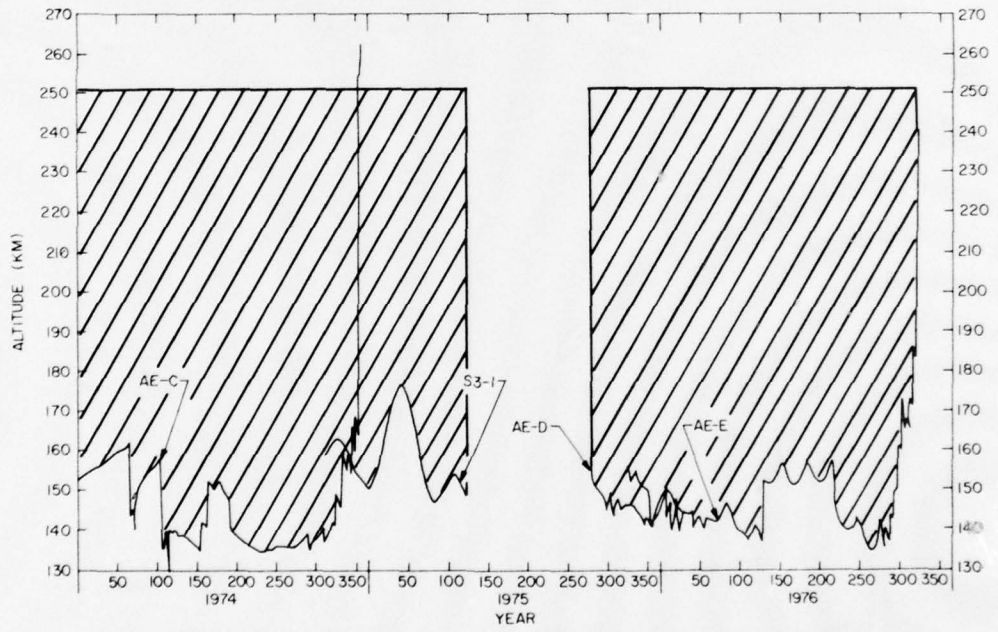

Figure 1. Distribution of Density Data in an Altitude-Time Coordinate System

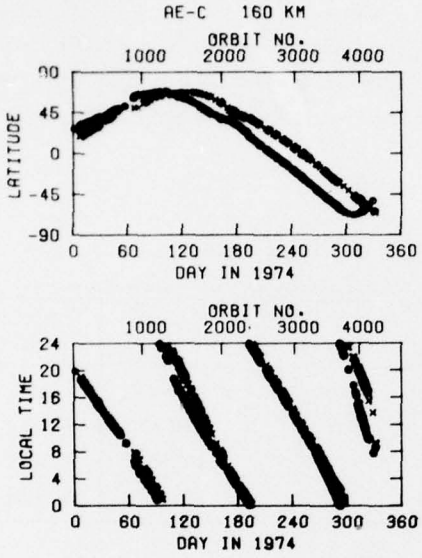

Figure 2a. Latitude and Local Time Distribution for AE-C 160 km Data

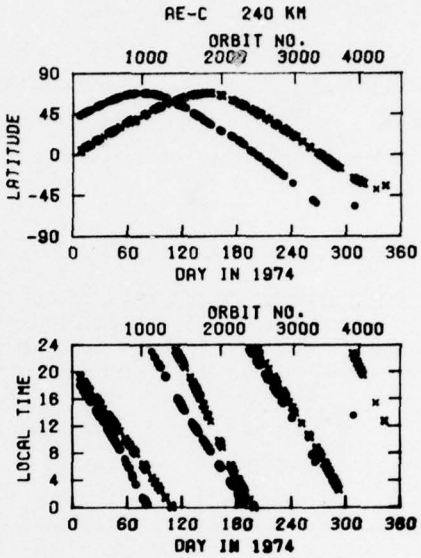

Figure 2b. Latitude and Local Time Distribution for AE-C 240 km Data

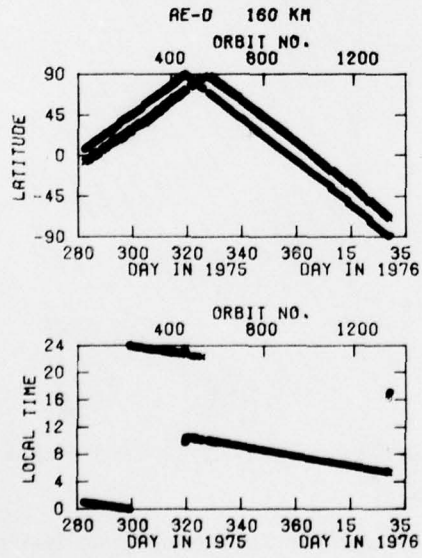

Figure 2c. Latitude and Local Time Distribution for AE-D 160 km Data

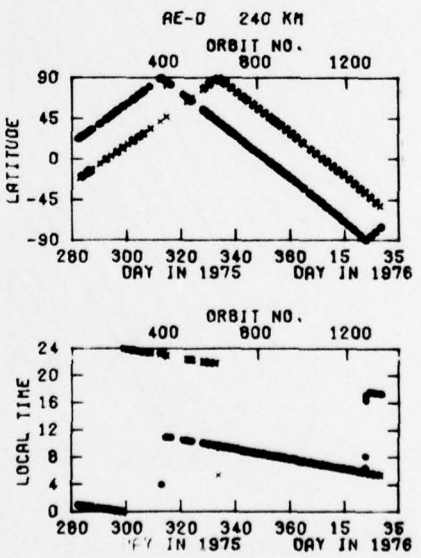

Figure 2d. Latitude and Local Time Distribution for AE-D 240 km Data

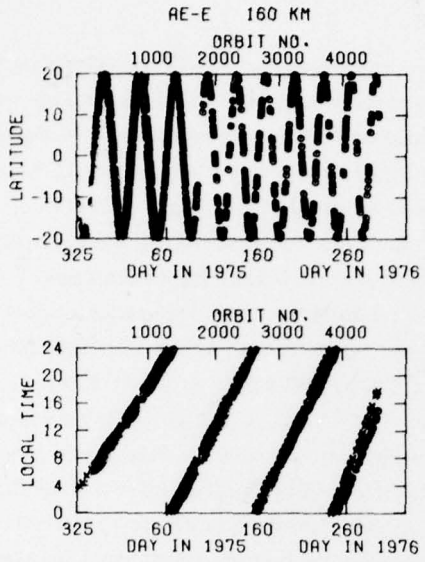

Figure 2e. Latitude and Local Time Distribution for AE-E 160 km Data

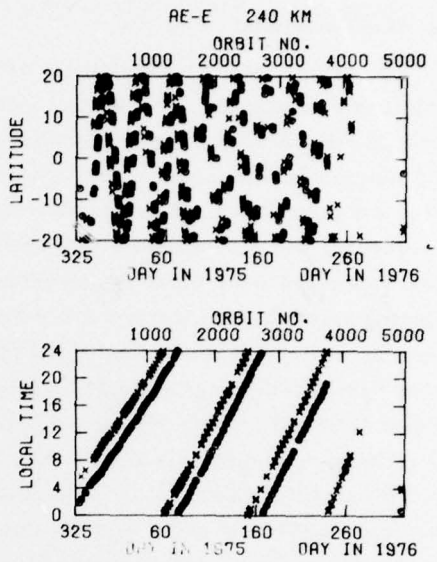

Figure 2f. Latitude and Local Time Distribution for AE-E 240 km Data

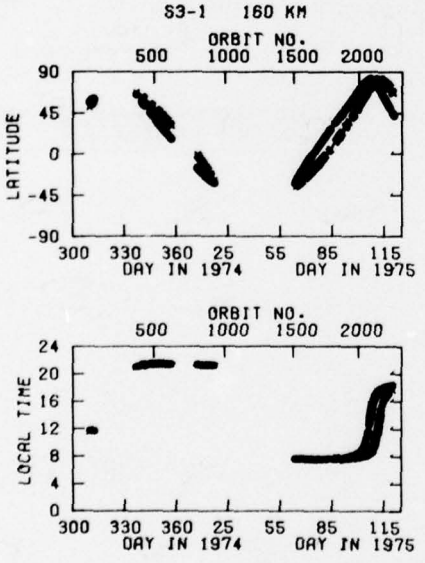

Figure 2g. Latitude and Local Time Distribution for S3-1 160 km Data

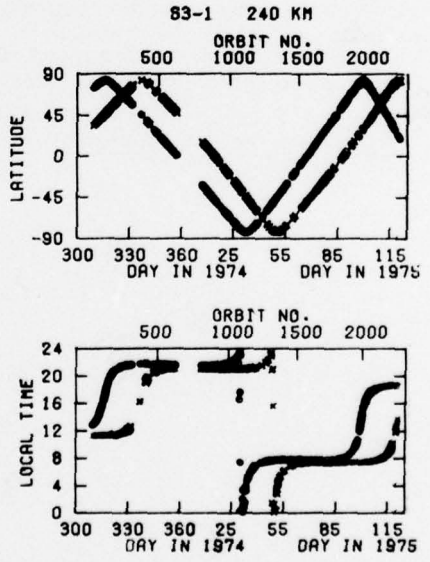

Figure 2h. Latitude and Local Time Distribution for S3-1 240 km Data

2.2 Drag Measurement

The accelerometer experiment provides extremely accurate measurements of orbital accelerations. Three single-axis instruments mounted orthogonally were flown on each AE satellite. Operating principles of this experiment have been given by Champion and Marcos.[7] S3-1 carried a single-axis sensor essentially identical to the AE instrument. The sensitive axis was aligned to the flight direction. A one-quarter sec sample-time was used for each instrument. Drag accelerations were separated from noise accelerations by numerical filtering techniques.[8] For spinning orbit data the errors are estimated as follows: area-to-mass uncertainty is ± 1%, attitude error is negligible (only ram point values are used), and filtering error varies from negligible at perigee to ± 2% at 200 km to ± 5% at 250 km. For despun orbit data (AE only) the sensors are at 45° ± 2° to the velocity vector and the attitude uncertainty is ± 2%. For both spinning and despun data there may be a ± 10% error in the assumed free molecular flow drag coefficient value of 2.2. The drag coefficient error and area-to-mass uncertainty constitute systematic errors. Hence the random error in measurement of density variations on a spinning satellite varies from negligible at perigee to ± 5% at 250 km. For the AE despun mode data, due to the accelerometer alignment with respect to the velocity vector and the accuracy of the attitude control system there is an additional ± 2% error. This could be alleviated by aligning the accelerometer sensitive axis with the velocity vector or by a higher accuracy attitude determination system.

7. Champion, K.S.W., and Marcos, F.A. (1973) The triaxial accelerometer system on Atmosphere Explorer, Radio Sci. 8:263.

8. Noonan, J.P., Fioretti, R.W., and Hass, B. (1975) Digital Filtering Analysis Applied to the Atmosphere Explorer-C Satellite MESA Accelerometer Data, AFCRL-TR-75-0293.

2.3 Data Base

Density values calculated at 5-km intervals were stored in the data base. Associated with each point is the corresponding J71 and MSIS model value, ephemeris data, solar flux, and K_p value. A histogram of the data distribution as a function of geographic latitude for each satellite is given in Figures 3a through 3d. These figures show the number of data points obtained in each 10° latitude band. The percentages of the total amount of data (combining the four sets) in the latitude bands $0 \pm 20°$, $|20\text{-}50°|$ and $|70\text{-}90°|$ are 47%, 25%, and 11% respectively. The large amount of near equatorial data is due to the low inclination of AE-E and the precession of perigee for the other satellites as indicated by Figure 1. The data above $|70°|$ are provided by AE-D and S3-1. Although relatively small in percentage of total data, 12,822 points were obtained at these latitudes. Figures 4a through 4d show the data distribution as a function of local time, giving the number of points within each 1-hr interval. The figures show excellent local time coverage provided by AE-C and -E. The distribution of data with respect to geomagnetic activity is shown in Figures 5a through 5d. These plots give the number of measurements during which the 3-hourly K_p index (with a 6-hr lag) fell within specific 1-unit intervals. Approximately 20% of all the data occur during conditions when the average K_p is greater or equal to 4_o. The relative frequency distribution for K_p values is similar to that obtained from a study for the period 1932-1971.[9] In Figures 6a through 6d distribution of data with solar flux is shown. These plots give the number of measurements during which the $F_{10.7}$ value (with a 1-day lag) fell within specific five solar flux unit intervals. It can be seen that the data base was obtained mainly during conditions of very low solar flux. Only about 4% of the data occur on days with $F_{10.7} > 100$. An example of the data base is given by showing results obtained at the altitude of 180 km for each satellite. Figures 7a through 7d show these density data, the latitude at which each data point was obtained, the ratio of measured density to the J71 model, and the K_p index.

9. Cage, A. L., and Zawalick, E. J. (1972) A Discussion of the Geomagnetic Indices K_p and A_p, 1932 to 1971, AFCRL-72-0693.

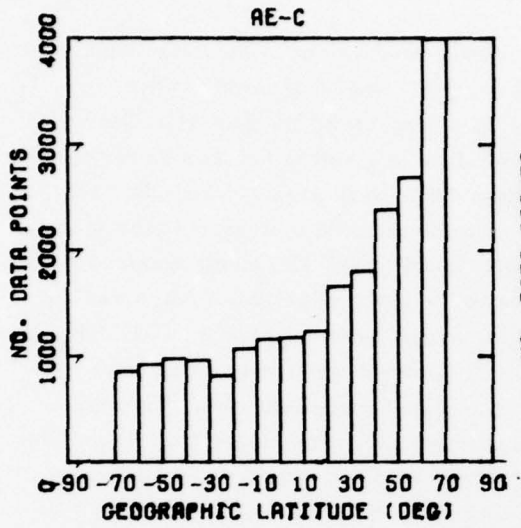

Figure 3a. Histogram of AE-C Data Distribution as a Function of Geographic Latitude

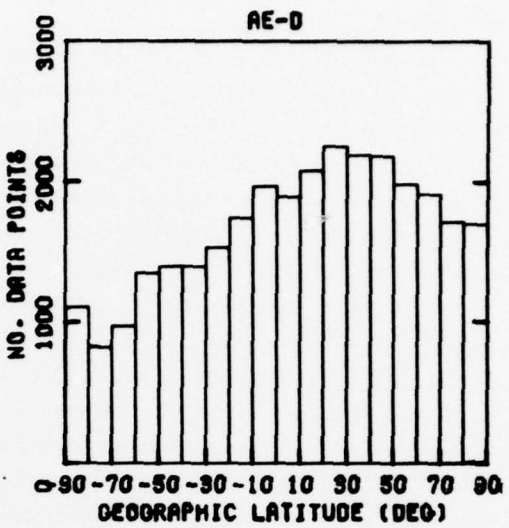

Figure 3b. Histogram of AE-D Data Distribution as a Function of Geographic Latitude

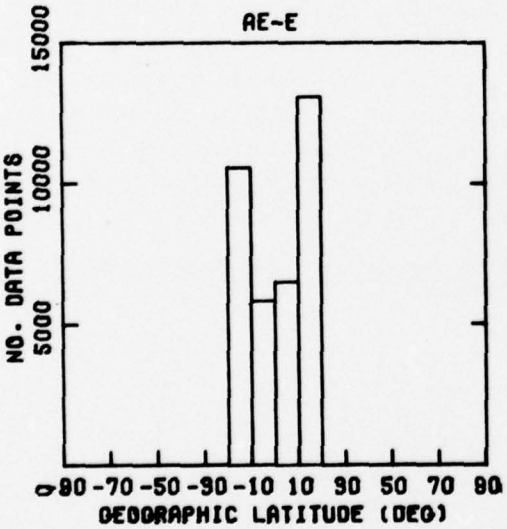

Figure 3c. Histogram of AE-E Data Distribution as a Function of Geographic Latitude

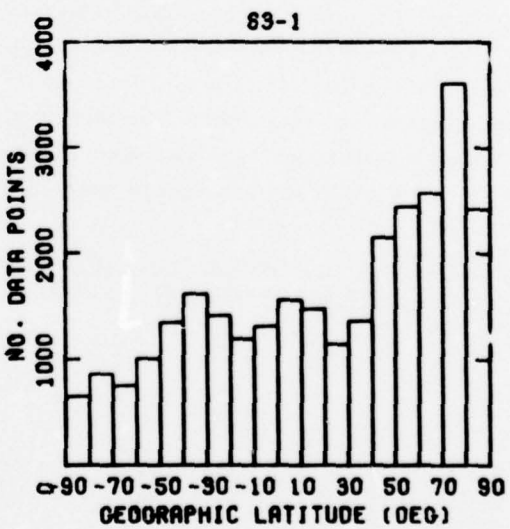

Figure 3d. Histogram of S3-1 Data Distribution as a Function of Geographic Latitude

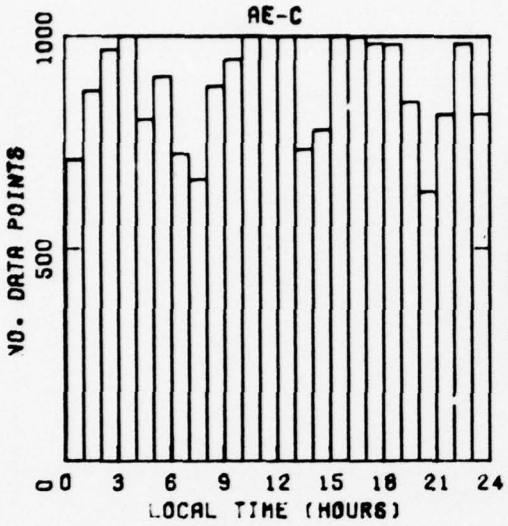

Figure 4a. Histogram of AE-C Data Distribution as a Function of Local Time

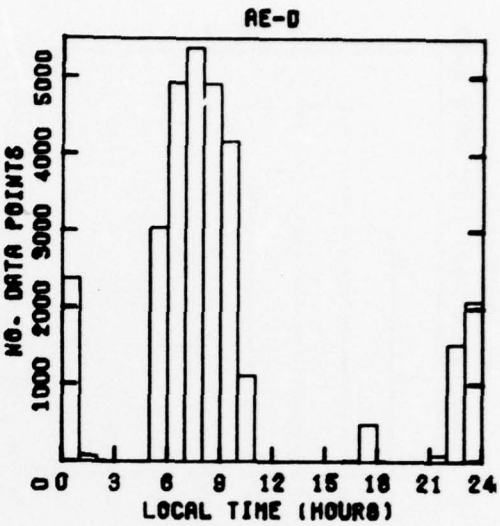

Figure 4b. Histogram of AE-D Data Distribution as a Function of Local Time

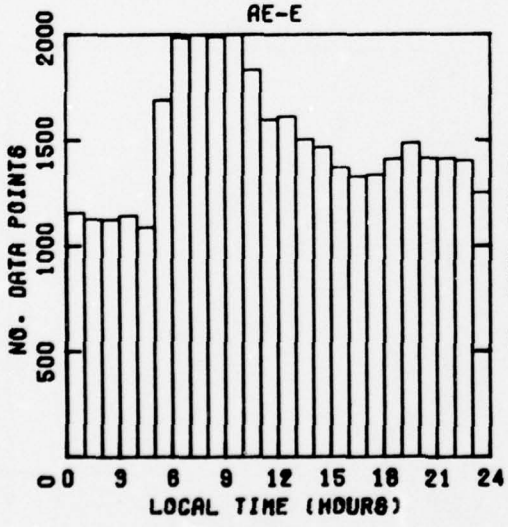

Figure 4c. Histogram of AE-E Data Distribution as a Function of Local Time

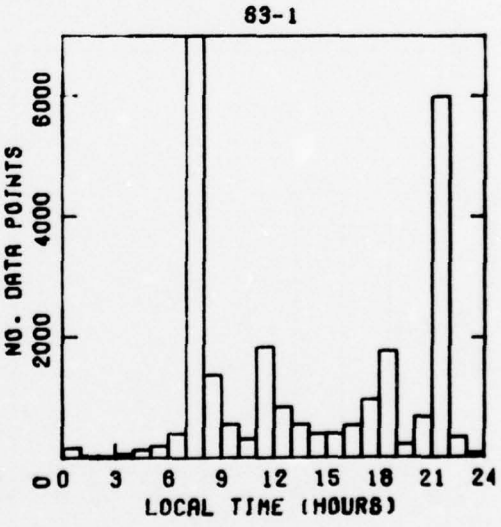

Figure 4d. Histogram of S3-1 Data Distribution as a Function of Local Time

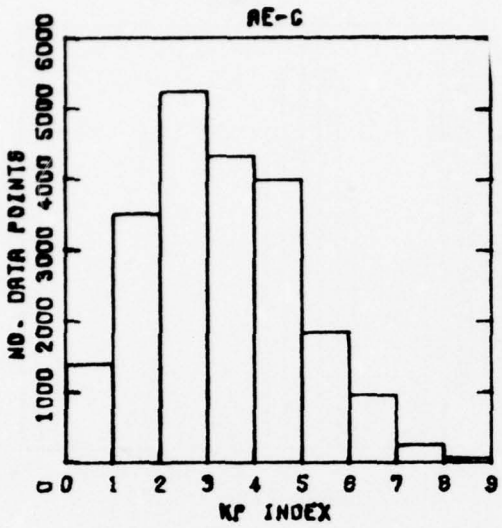

Figure 5a. Histogram of AE-C Data Distribution as a Function of Geomagnetic Activity

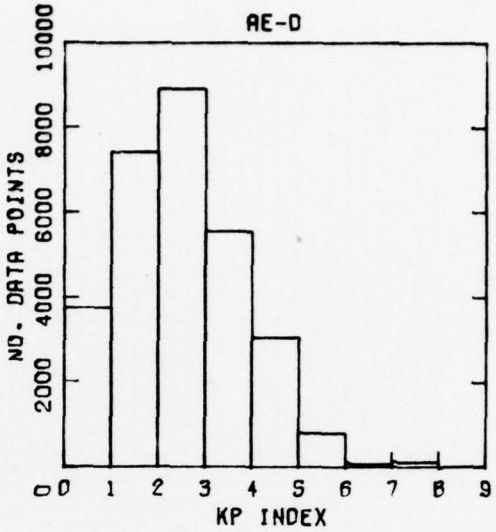

Figure 5b. Histogram of AE-D Data Distribution as a Function of Geomagnetic Activity

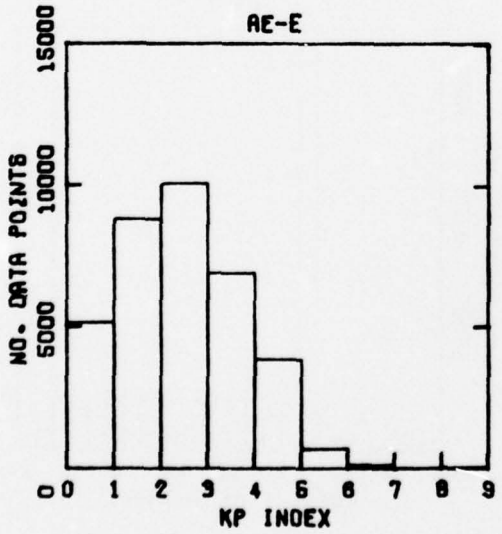

Figure 5c. Histogram of AE-E Data Distribution as a Function of Geomagnetic Activity

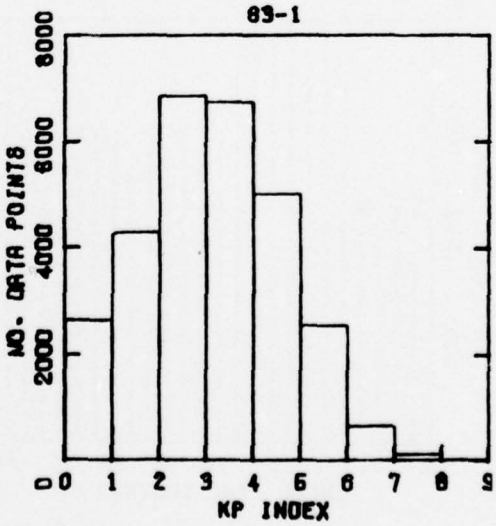

Figure 5d. Histogram of S3-1 Data Distribution as a Function of Geomagnetic Activity

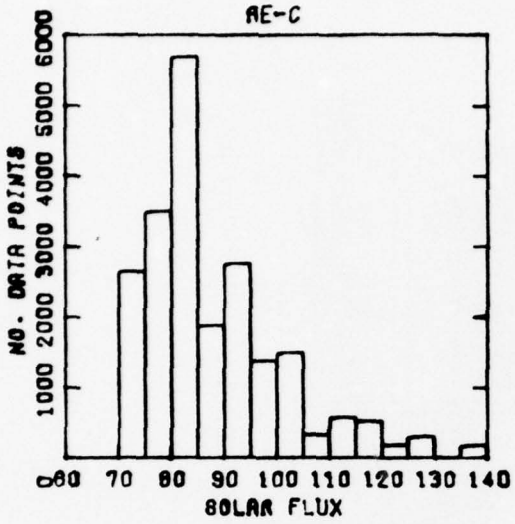

Figure 6a. Histogram of AE-C Data Distribution as a Function of Solar Flux

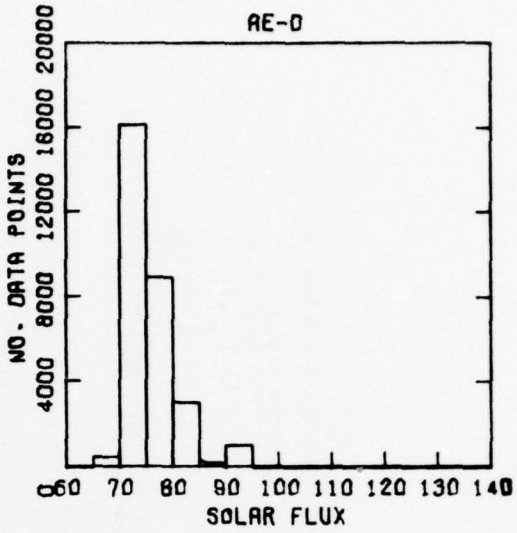

Figure 6b. Histogram of AE-D Data Distribution as a Function of Solar Flux

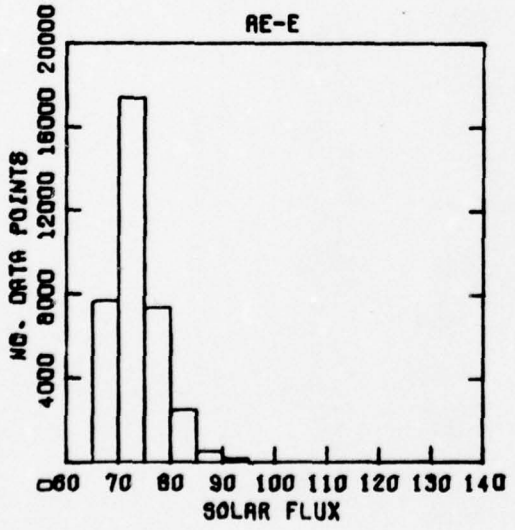

Figure 6c. Histogram of AE-E Data Distribution as a Function of Solar Flux

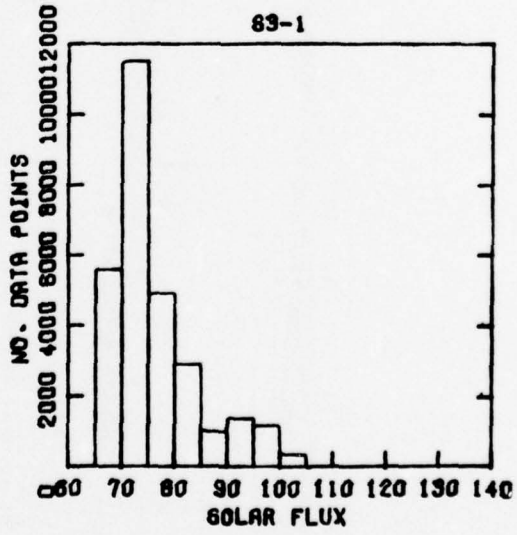

Figure 6d. Histogram of S3-1 Data Distribution as a Function of Solar Flux

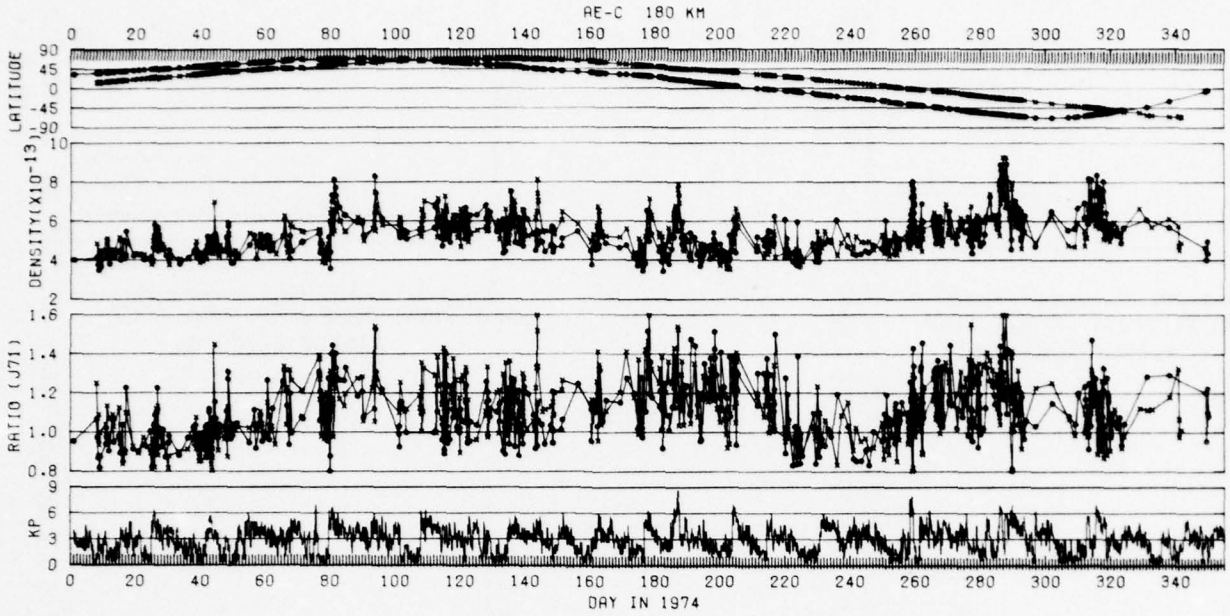

Figure 7a. AE-C Data Base at 180 km: Latitude, Density (g/cm^3) Ratio to J71 Model and K_p as a Function of Time

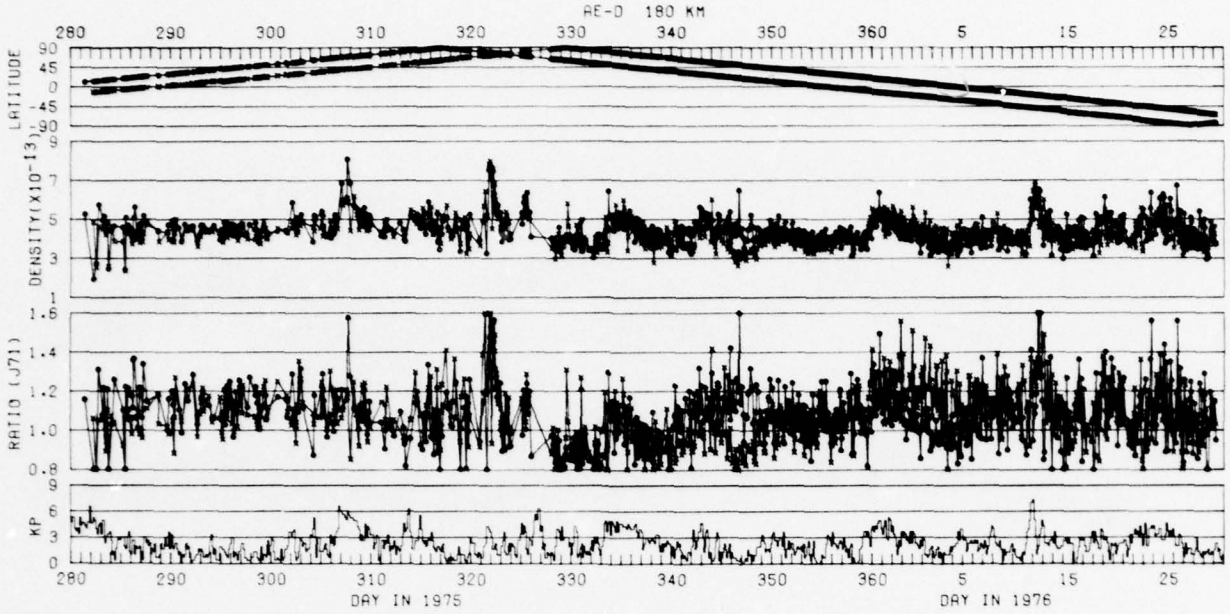

Figure 7b. AE-D Data Base at 180 km: Latitude, Density (g/cm^3) Ratio to J71 Model and K_p as a Function of Time

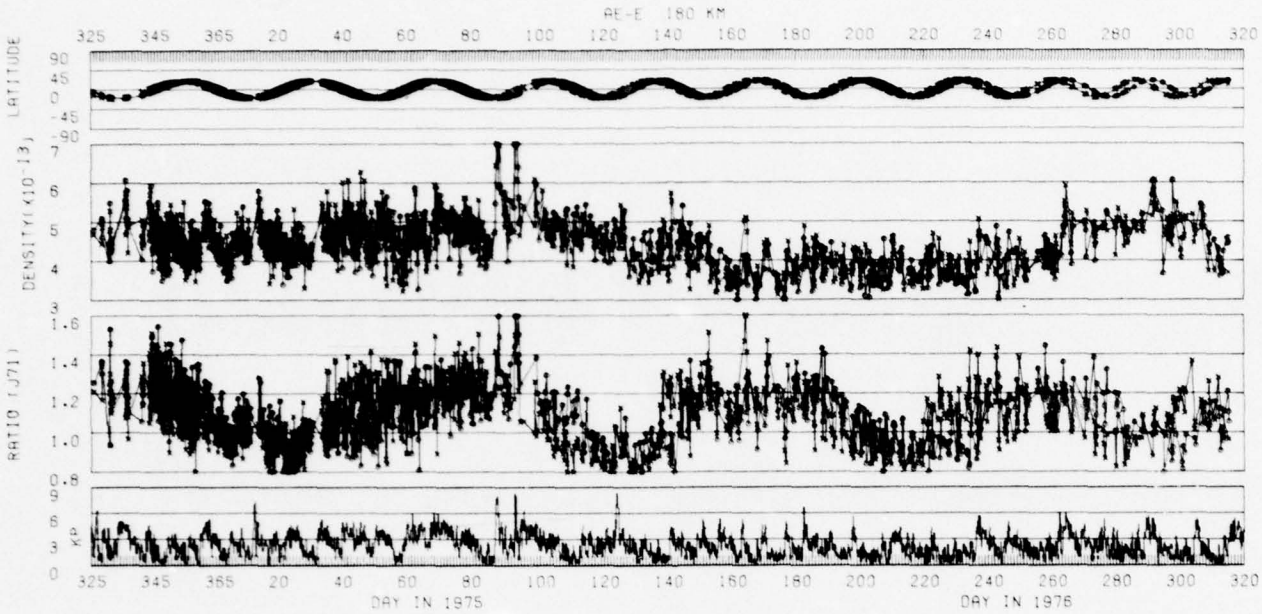

Figure 7c. AE-E Data Base at 180 km: Latitude, Density (g/cm^3) Ratio to J71 Model and K_p as a Function of Time

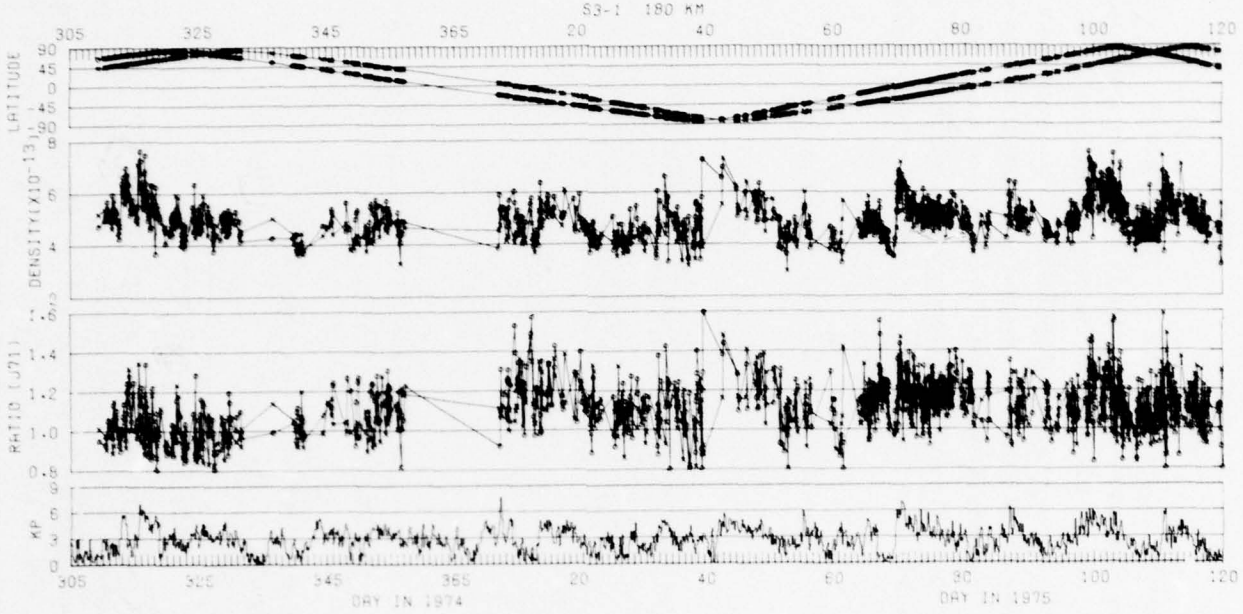

Figure 7d. S3-1 Data Base at 180 km: Latitude, Density (g/cm^3) Ratio to J71 Model and K_p as a Function of Time

3. RESULTS

3.1 Statistical Properties

The measured density values have been statistically analyzed in relation to the J71 and MSIS models. The normal distribution is completely determined by two constants: the mean locates the center of the distribution, and the standard deviation measures the spread or variation of the individual measurements. Extreme deviations from models are of particular interest to potential Air Force users, hence departures of frequency distributions of the data from a normal distribution have also been calculated. The following moments of x, which represent the percent departure of the data from the model values have been determined:[10]

Mean value ($\bar{x}$)

$$\bar{x} = \sum_{i=1}^{N} \frac{x_i}{N} , \tag{1}$$

where x_i is the percent deviation of the i^{th} density measurement from the model and N is the total number of data points,

Standard deviation (S)

$$S = \left[\sum_{i=1}^{N} \frac{(x_i - \bar{x})^2}{N-1} \right]^{1/2} . \tag{2}$$

For a normal distribution about 68.3% of the data fall in the interval $\bar{x} \pm S$, 95.5% are within $\bar{x} \pm 2S$, and 99.73% are within $\bar{x} \pm 3S$,

Skewness or, third moment about the mean, ($\sqrt{b_1}$)

$$\sqrt{b_1} = \frac{1}{S^3} \sum_{i=1}^{N} \frac{(x_i - \bar{x})^3}{N} . \tag{3}$$

The skewness, a measure of non-symmetry, will be positive if the lower values of x are closer to the mean than the higher values, that is, if the distribution has a large tail to the right (positive side) of the mean. In this case, large positive contributions $(x-\bar{x})^3$, when x exceeds $\bar{x}$, will dominate the smaller negative contributions obtained when x is less than $\bar{x}$. Negative skewness indicates that the lower tail is the extended one. The factor $\frac{1}{S^3}$ renders this measure independent

10. Snedecor, G. W., and Cochran, W. G. (1967) Statistical Methods, Iowa State University Press, Iowa.

of scale. If $\sqrt{b_i}$ is zero, the distribution is symmetric with respect to the mean. The criterion for 95% confidence that the non-zero skewness observed is not due to sampling error is $|\sqrt{b_i}| > (1.96)\sqrt{\frac{6}{N}}$, where N is the number of sampling points.

Kurtosis or fourth moment about the mean, (b_2)

$$b_2 = \frac{1}{S^4} \sum_{i=1}^{N} \frac{(x_i - \bar{x})^4}{N} . \tag{4}$$

For a normal distribution b_2 has a value of 3. Values of b_2 greater than 3 indicate an excess of values near the mean and far from the mean with a corresponding depletion of intermediate values of the distribution curve. For values of $b_2 < 3$ the distribution curve has a flatter top than normal. The criterion for 95% confidence that the kurtosis observed is in fact different from 3 and not due to sampling error is that

$$|b_2 - 3| > (3.92)\sqrt{\frac{6}{N}} .$$

3.2 Frequency and Probability Distribution

Graphical representations of frequency distributions of percent differences from models have been developed. These histograms are shown for each set of satellite data. This separation by satellite permits some intercomparison as a function of the different geophysical conditions appropriate to each set of data. Planned studies of atmospheric variability related to geomagnetic activity, latitude, longitude, season, and the semi-annual variation will use the data base in a unified format.

Histograms are shown in Figures 8a through 8d for each set of satellite data (at all altitudes) compared to the J71 model. The plots show the percentage of the total number of data points falling within each 1% model deviation interval. The total number of points is given at the bottom of the box in the upper right hand corner of each figure. A normal distribution curve is superimposed as a solid curve on each histogram. Deviations from the normal curve are observed with each set of satellite data. Values for the coefficients in Eqs. (1) to (4) are provided in the right hand corner of each figure. The mean values fall within the range $6.9 \pm 2.5\%$. The standard deviations are within the range $16.1 \pm 0.6\%$. The skewness coefficient is positive for all cases indicating an excess of large positive deviations relative to a normal distribution. The kurtosis has a value greater than 3 for each case. These properties of the third and fourth moments are statistically confirmed since $1.96\sqrt{\frac{6}{N}}$ and $3.92\sqrt{\frac{6}{N}}$ are less than $\sqrt{b_1}$ and $|b_2 - 3|$ respectively for each case.

Figures 9a through 9d show the same data as in Figures 8a through 8d, but compared to the MSIS model. This model gives better agreement to the average measured absolute density values than J71. The mean falls within 2.9 ± 3.6% for each set of data. Standard deviations are also slightly lower, falling within the range 14.1 ± 1.7%. As with the data in Figures 8a through 8d, the skewness coefficient is always positive and the kurtosis is always greater than 3. No trend was found for these coefficients in comparing the data in Figures 8a through 8d and 9a through 9d.

The MSIS model predicts density values which are on the average 4% lower than those of the J71 models. Since the drag coefficient may differ systematically from its assumed value of 2.2 by about 10%, it cannot be determined which model more accurately predicts the absolute density.

An earlier study[11] comparing OV1-15 satellite accelerometer data to J71 found an average departure of about -7% from the model. These data were obtained for an average solar flux of 145 units. However, it cannot be determined whether the J71 model has a systematic error with respect to solar flux because of drag coefficient uncertainties. OV1-15 had an L/D≈2 compared to AE which had an L/D≈1. For the higher L/D the theoretical value of C_D is higher by about 10%.[12]

Cumulative frequency distribution curves are another useful means of displaying the deviations of the measured data from a normal distribution. Figures 10a through 10d show the results of Figures 8a through 8d plotted in this alternate format. The ordinate of a point on the curve gives the percent of the total data which deviates from the model by a percent less than or equal to the value of the abscissa. The ordinate scale at the right gives the cumulative percent in terms of standard deviations. These curves can be used to estimate the amount of expected large deviations from a model. For example, approximately 2.3% of all the AE-C data differ from the J71 model by between -80% and -20% and approximately 2.3% of this same data differ from the model by more than 45%. The normal distribution shows a linear dependence in this type plot and is shown as a solid line.

---

11. Marcos, F.A., and Champion, K.S.W. (1972) Variations of the neutral atmospheric density at low satellite altitudes, Proc. International Conf. on Aerospace and Aeronautical Meteorology, Washington, D.C.

12. Karr, G.A., and Smith, R.E. (1972) Influence of satellite aerodynamics on atmospheric density determination, Proc. International Conf. on Aerospace and Aeronautical Meteorology, Washington, D.C.

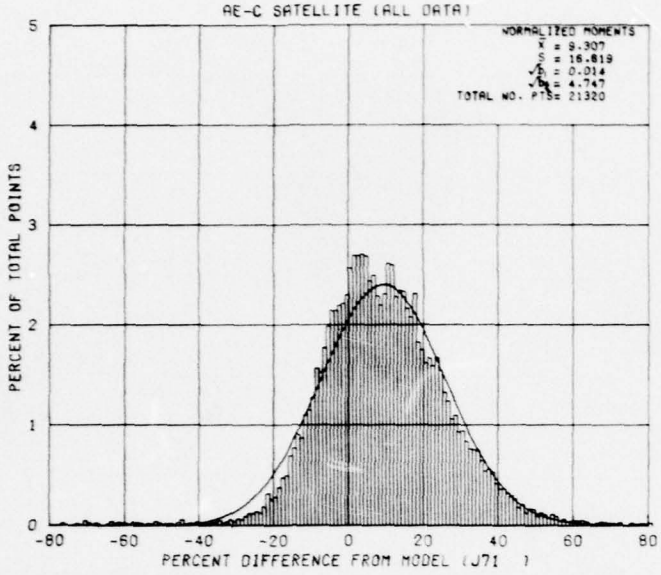

Figure 8a. Frequency Distribution of Percent Difference of AE-C Data from J71 Model

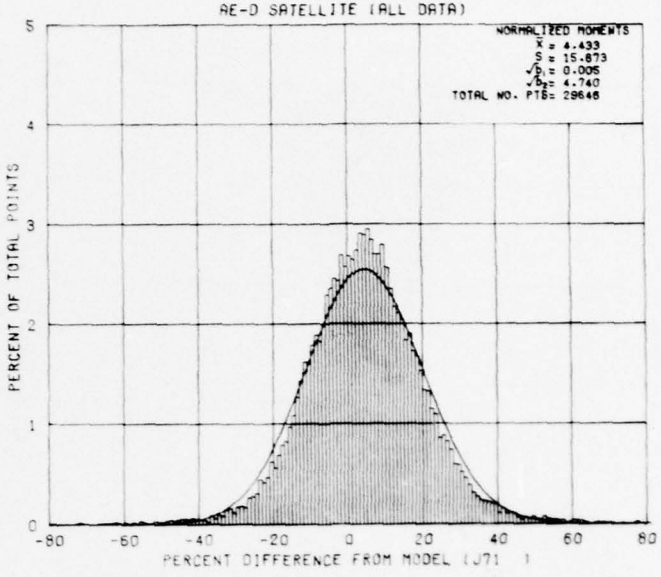

Figure 8b. Frequency Distribution of Percent Difference of AE-D Data from J71 Model

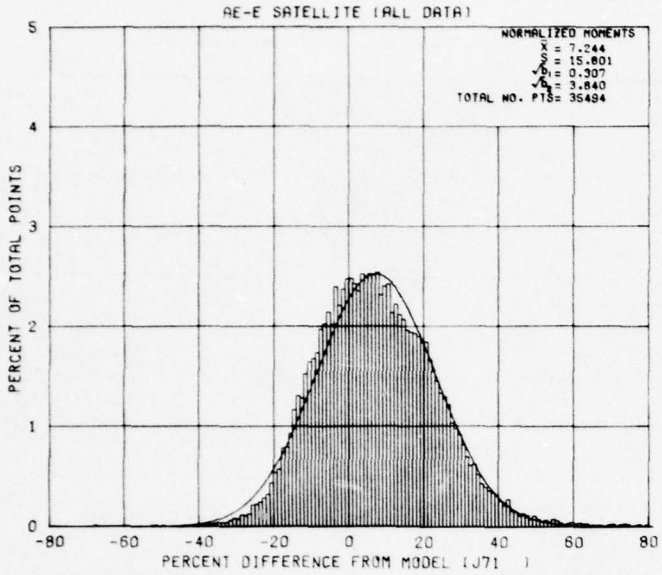

Figure 8c. Frequency Distribution of Percent Difference of AE-E Data from J71 Model

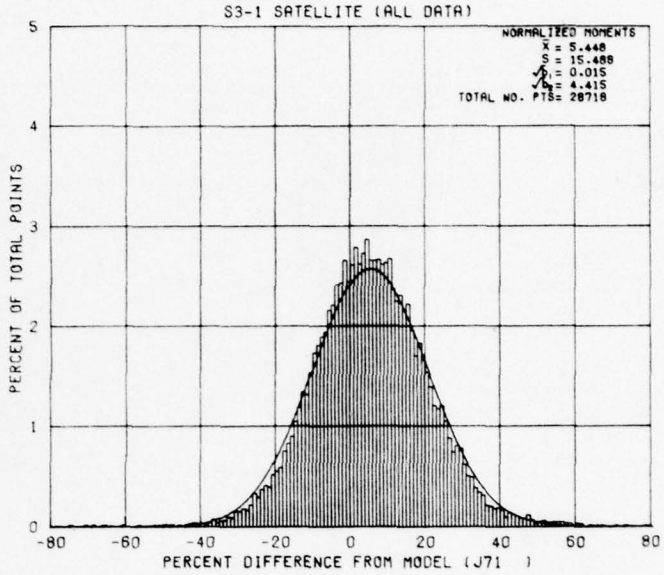

Figure 8d. Frequency Distribution of Percent Difference of S3-1 Data from J71 Model

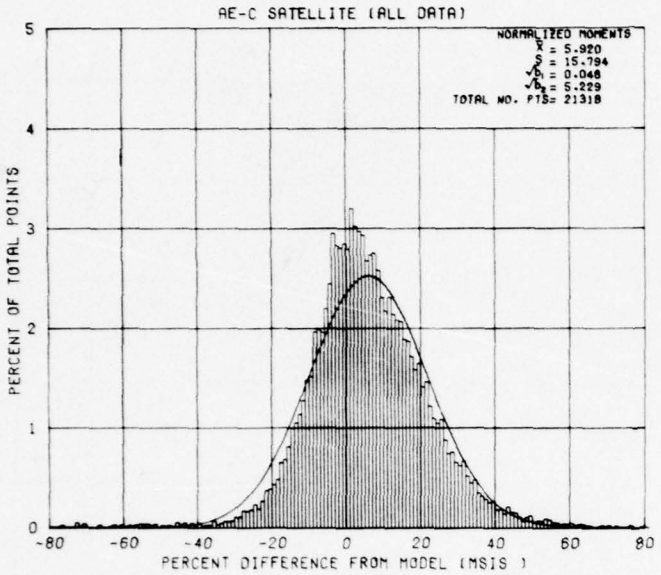

Figure 9a. Frequency Distribution of Percent Difference of AE-C Data from MSIS Model

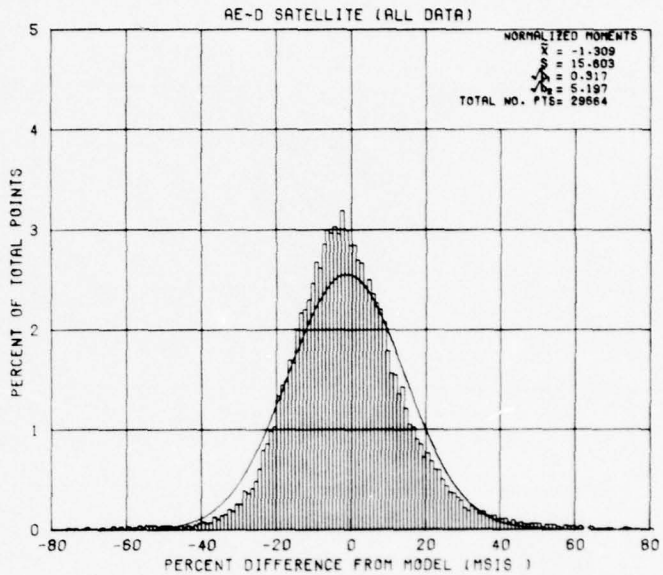

Figure 9b. Frequency Distribution of Percent Difference of AE-D Data from MSIS Model

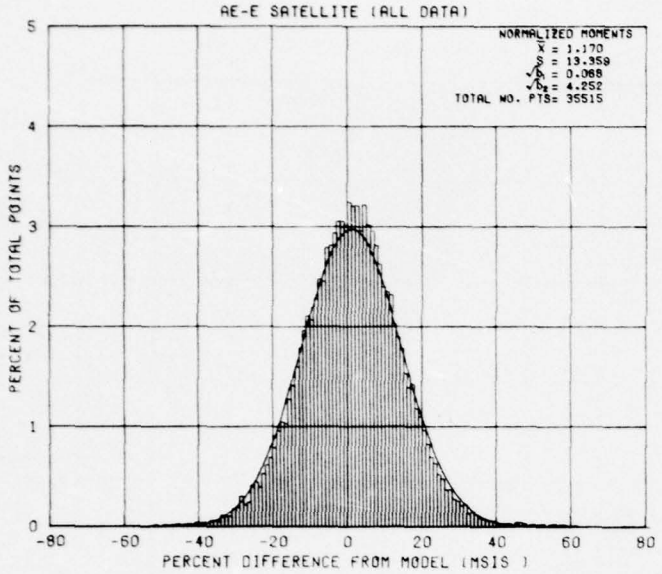

Figure 9c. Frequency Distribution of Percent Difference of AE-E Data from MSIS Model

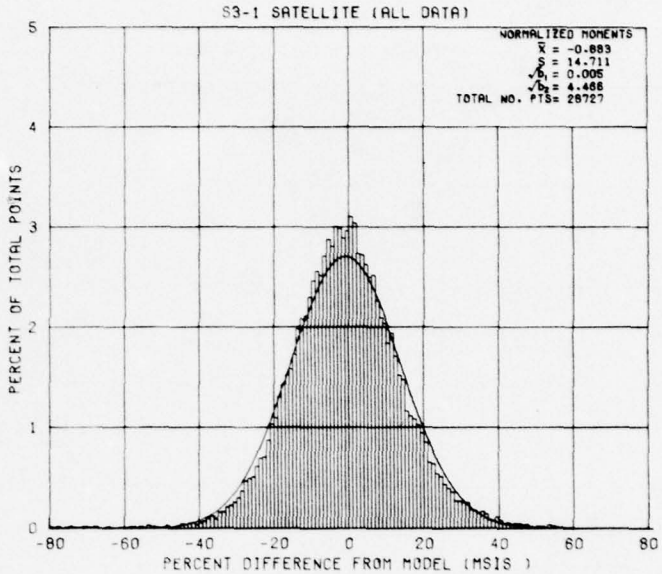

Figure 9d. Frequency Distribution of Percent Difference of S3-1 Data from MSIS Model

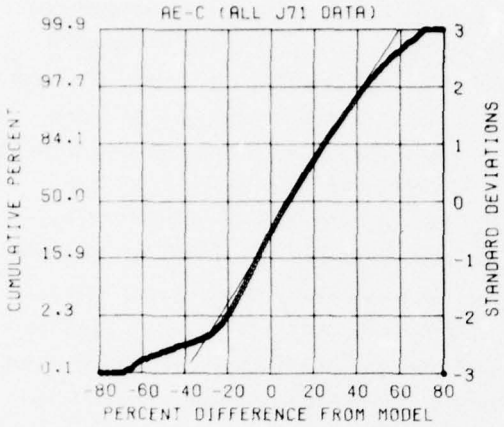

Figure 10a. Probability Distributions for AE-C Data Shown as Percent Departure from the J71 Model

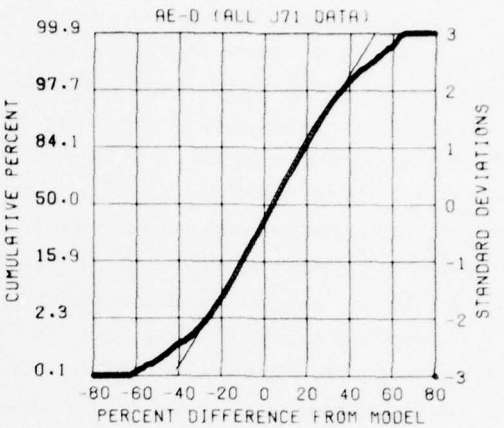

Figure 10b. Probability Distributions for AE-D Data shown as Percent Departure from the J71 Model

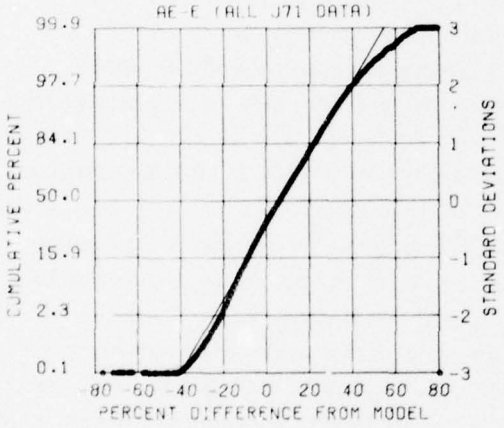

Figure 10c. Probability Distributions for AE-E Data Shown as Percent Departure from the J71 Model

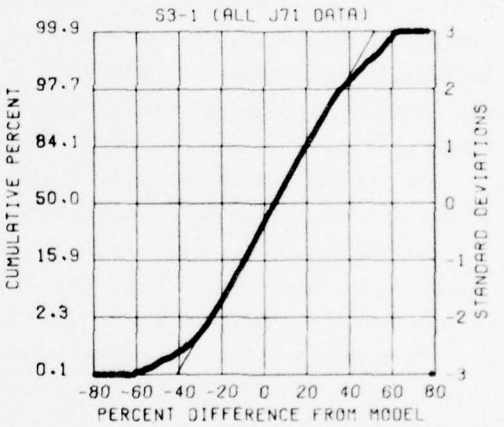

Figure 10d. Probability Distributions for S3-1 Data Shown as Percent Departure from the J71 Model

3.3 Data as a Function of Geomagnetic Activity and Latitude

Frequency distributions were made for data obtained at different levels of geomagnetic activity and at different geographic latitudes. The S3-1 data were used since it has the best distribution with respect to K_p and latitude. The data are first displayed as a function of geomagnetic activity only. Three groups of data were formed according to the K_n index (with a 6-hr lag). Group A included measurements obtained with the condition $K_p \leq 3_-$. Groups B and C were for data with $K_p \geq 4_o$ and $K_p \geq 5_o$ respectively. The range $4_- \geq K_p \geq 3_-$ was omitted to provide a larger difference between Groups B and C. Next the data were separated into 30° latitude bins. The mean and moments about the mean were calculated for Group A and B.

Results obtained when the data are separated by K_p only are shown in Figures 11a through 11c and 12a through 12c. These figures show the frequency distributions for data compared to J71 and MSIS respectively. The results are summarized as follows:

(1) Mean value: The actual average measured increase in density for Group B relative to Group A is 18%. For Group C relative to Group A it is 24%. The J71 Group B and C ratios are about 1.5% less than those of Group A. The MSIS Group B and C ratios are about 5% greater than those of Group A. Hence the J71 model provides a more accurate representation of the geomagnetic activity effect. The MSIS model underestimates it by about 5% probably because this model uses a daily average K_p value to estimate the density enhancement related to geomagnetic activity.

(2) Standard deviation: For all six cases S is within 15.3 ± 1%. The largest values of S occur with the Group C data for both models.

(3) Skewness: An increase in b_1 with increasing K_p is observed in Figures 11a through 11c and 12a through 12c. This is indicative of a relative increase in the number of positive deviations from the mean with increasing K_p.

(4) Kurtosis: The value of b_2 decreases as K_p increases. For both Group A sets $b_2 = 5.3$. For Groups B and C $3.4 \leq b_2 \leq 3.9$. With increasing K_p the peak of the distribution flattens out while the number of intermediate values increases.

The Group A and Group B data were next separated into 30° latitude bins. Group C data were not included in this study because a relatively small number of points were obtained at high southern latitudes. Calculated values of the mean and moments about the mean have been tabulated for this study and are shown in Table 2. Table 2 shows data for Groups A and B (low and high K_p conditions, respectively) relative to both the J71 and MSIS models. For low K_p conditions (Group A) the MSIS model appears to provide a more accurate depiction of the latitudinal structure; $\bar{x}$ is within -4.3 ± 2.6% for MSIS and 8.3 ± 5.9% for J71. In general, J71 overestimates the average geomagnetic activity effect by about 4% from -60° to -30° and accurately depicts it from +30° to -90°. MSIS values are about 6% low from -30° to -60° and

about 3% low in the latitude intervals -60° to +30° and +60° to +90°. The largest standard deviation occurs at -30° to -60° for both models. However, relatively low values occur at +30° to +60°. As was found in Figures 11a through 11c and 12a through 12c, skewness increases with increasing K_p and kurtosis decreases.

Table 2. Mean and Standard Deviation as Percent Deviation from J71 and MSIS Models for S3-1 Low and High K_p Data Group vs Latitude

Moments for S3-1 All Data (J71 Model)									
	Latitude Min	Latitude Max	K_p Min	K_p Max	Number of Pts	Avg. Value	Standard Deviation	Skewness Coeff.	Kurtosis
Group A	-90	-60	0.0	2.5	988	4.7935	14.0539	-.0912	3.8518
	-60	-30	0.0	2.5	1717	8.5629	15.0697	-.3516	6.8126
	-30	0	0.0	2.5	1529	14.1795	18.6116	-.7964	6.1269
	0	30	0.0	2.5	1204	10.6487	16.6563	-.9783	7.7262
	30	60	0.0	2.5	2177	2.3865	14.8664	-.4084	5.2432
	60	90	0.0	2.5	3697	3.3115	13.2219	.2369	4.1379
Group B	-90	-60	4.0	9.1	396	11.1768	17.1003	.2438	3.6008
	-60	-30	4.0	9.1	1165	4.5446	18.6983	-.1148	4.0389
	-30	0	4.0	9.1	1180	10.0331	14.3865	-.5208	4.7926
	0	30	4.0	9.1	1424	6.8539	13.9825	.0447	2.9412
	30	60	4.0	9.1	1945	2.0985	13.5425	.3825	3.6517
	60	90	4.0	9.1	2163	3.3659	16.3584	.5577	4.2089

Total Number of Points = 19,585

Moments for S3-1 All Data (MSIS Model)									
	Latitude Min	Latitude Max	K_p Min	K_p Max	Number of Pts	Avg. Value	Standard Deviation	Skewness Coeff.	Kurtosis
Group A	-90	-60	0.0	2.5	988	-6.5091	12.8766	-.0822	3.6022
	-60	-30	0.0	2.5	1718	-3.7835	13.5575	-.0433	7.0258
	-30	0	0.0	2.5	1530	-1.6719	16.6452	-.4358	5.3455
	0	30	0.0	2.5	1204	-3.9028	14.7894	-.3016	7.9201
	30	60	0.0	2.5	2177	-6.9575	14.5492	-.0310	5.1573
	60	90	0.0	2.5	3697	-2.9872	13.4507	.1688	3.6690
Group B	-90	-60	4.0	9.1	396	1.3485	16.5364	.1776	3.0011
	-60	-30	4.0	9.1	1165	0.0288	17.5674	-.0234	4.3017
	-30	0	4.0	9.1	1180	4.6161	13.7908	-.3970	4.6085
	0	30	4.0	9.1	1424	3.2444	13.4583	.1157	2.8777
	30	60	4.0	9.1	1945	-0.0491	13.7986	.2281	2.9733
	60	90	4.0	9.1	2165	1.6072	16.1643	.1117	3.2651

Total Number of Points = 19,589

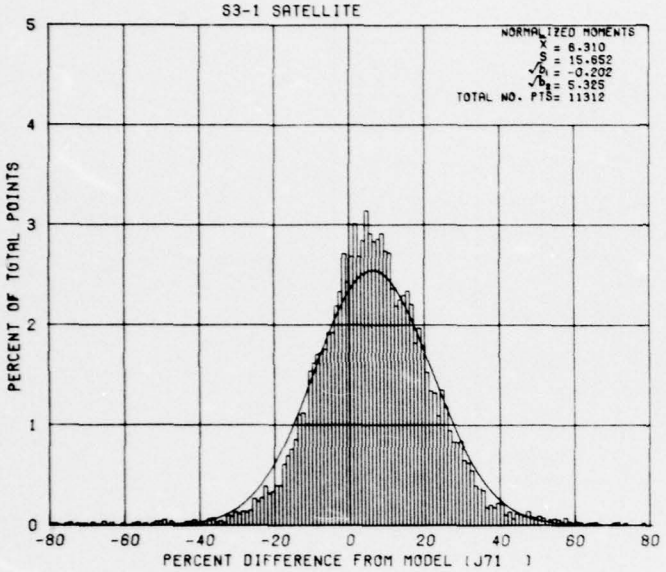

Figure 11a. Frequency Distribution of Percent Difference of S3-1 Data for $K_p < 3_-$ from J71 Model

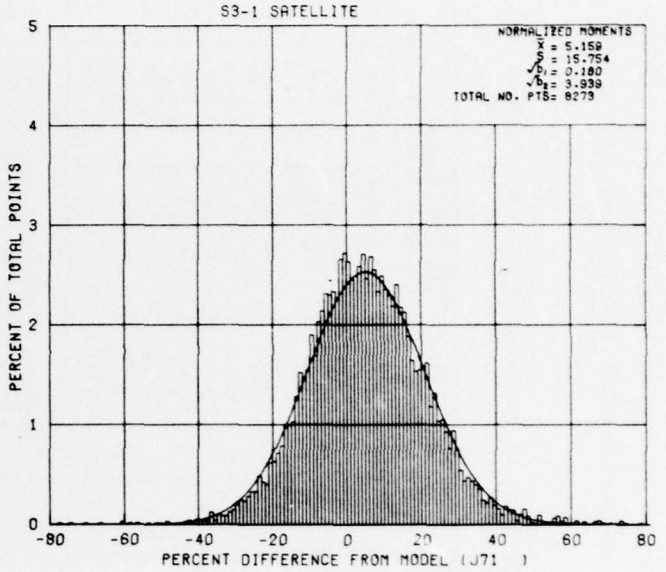

Figure 11b. Frequency Distribution of Percent Difference of S3-1 Data for $K_p \geq 4_o$ from J71 Model

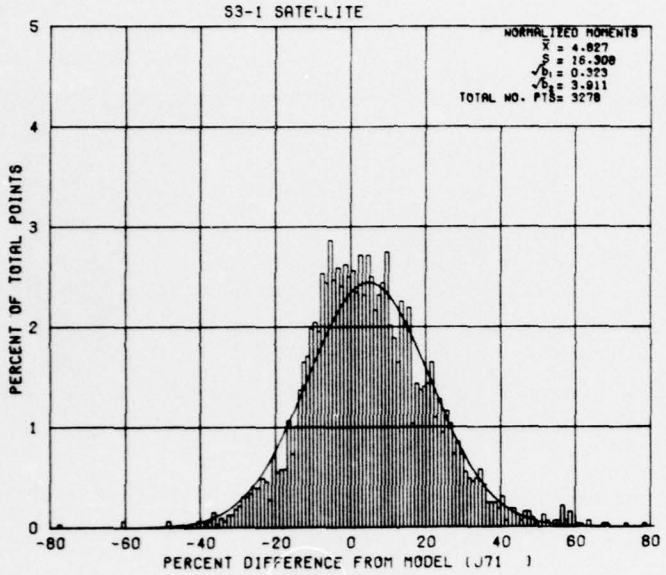

Figure 11c. Frequency Distribution of Percent Difference of S3-1 Data for $K_p \geq 5_o$ from J71 Model

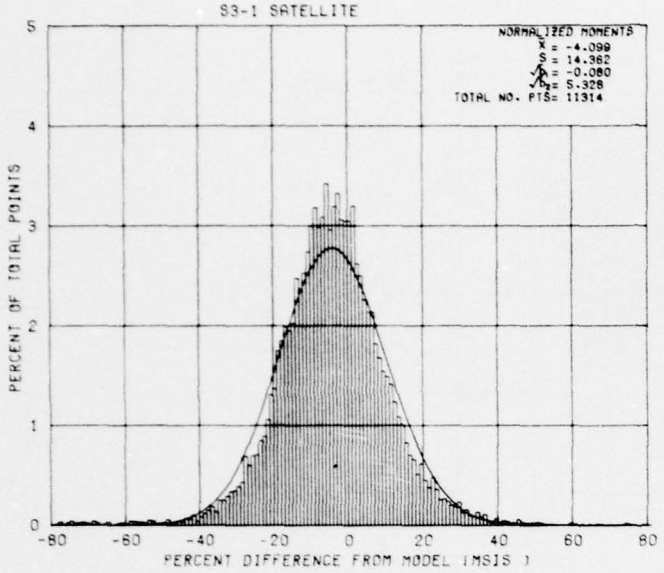

Figure 12a. Frequency Distribution of Percent Difference of S3-1 Data for $K_p < 3_-$ from MSIS Model

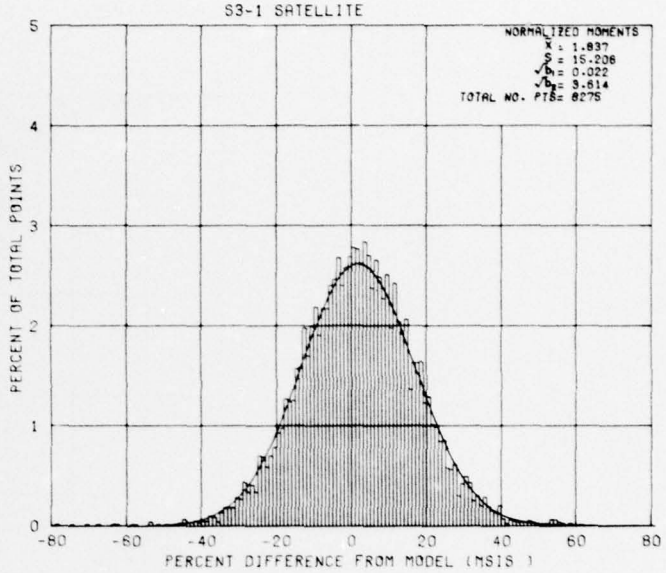

Figure 12b. Frequency Distribution of Percent Difference of S3-1 Data for $K_p \geq 4_o$ from MSIS Model

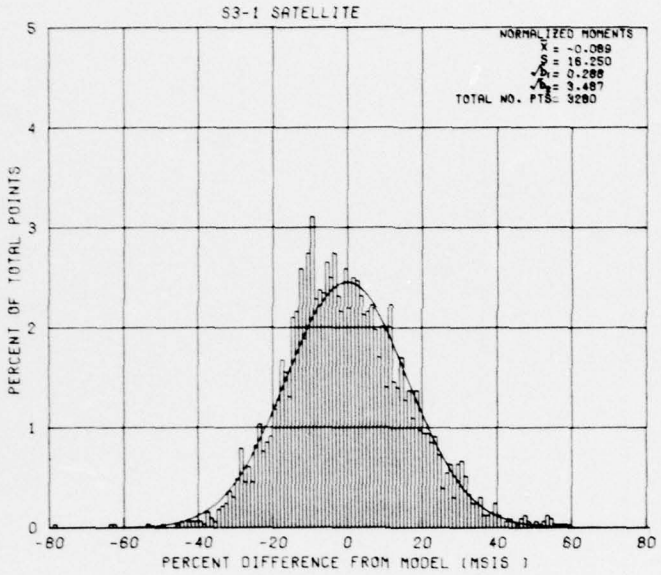

Figure 12c. Frequency Distribution of Percent Difference of S3-1 Data for $K_p \geq 5_o$ from MSIS Model

3.4 Altitude Dependence

Mean and standard deviation values were calculated for the ratio of data-to-model, and the average percent deviation from the model was plotted as a function of altitude. Values were computed at 5 km intervals using all data for each satellite. Figures 13a through 13d and 14a through 14d show results compared to J71 and MSIS respectively. Mean values are represented by crosses; standard deviations are shown as solid lines. The mean values with respect to J71 are between +6% (AE-D) and +15% (S3-1) at 160 km. Comparison is made at this altitude since below 160 km the number of data points decreases and varies significantly from satellite to satellite (see Figure 1). At 240 km $\bar{x}$ is between -2% (S3-1) and +4% (AE-E). With respect to MSIS $\bar{x}$ is between +4% (AE-D) and +10% (AE-C) at 160 km and -9% (S3-1) and -2% (AE-E) at 240 km. MSIS provides a particularly accurate representation of the AE-E data. The J71 scale heights are in general 10% too high below about 170 km. Above this altitude they are about 10% lower than the measured data. The MSIS scale heights are also about 10% too low. Standard deviations are about 15% at 160 km and increase to about 20% at 240 km. The increase is due to the approximately 5% filtering error in the data reduction at this altitude. The large standard deviation for S3-1 occurs below 160 km where there are relatively few data points.

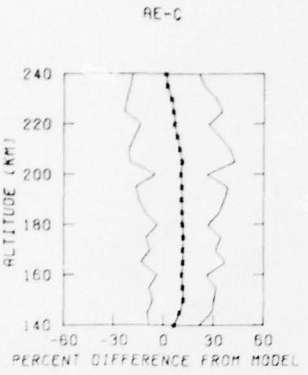

Figure 13a. Percent Deviation from the J71 Model of the Mean and Standard Deviations of AE-C Density Measurements vs Altitude

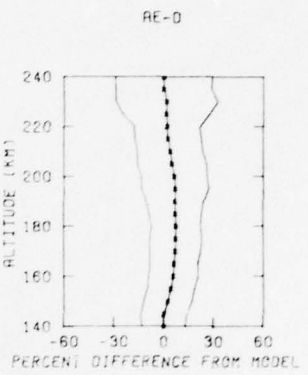

Figure 13b. Percent Deviation from the J71 Model of the Mean and Standard Deviations of AE-D Density Measurements vs Altitude

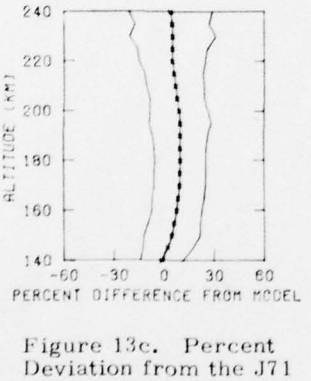

Figure 13c. Percent Deviation from the J71 Model of the Mean and Standard Deviations of AE-E Density Measurements vs Altitude

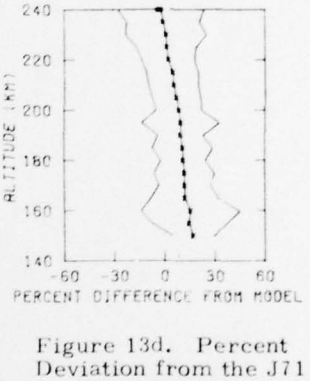

Figure 13d. Percent Deviation from the J71 Model of the Mean and Standard Deviations of S3-1 Density Measurements vs Altitude

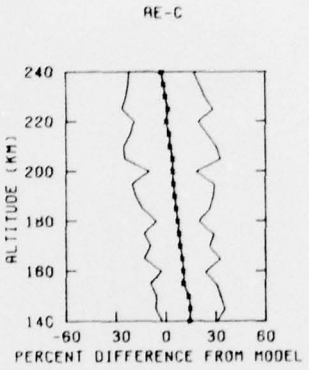

Figure 14a. Percent Deviation from the MSIS Model of the Mean and Standard Deviations of AE-C Density Measurements vs Altitude

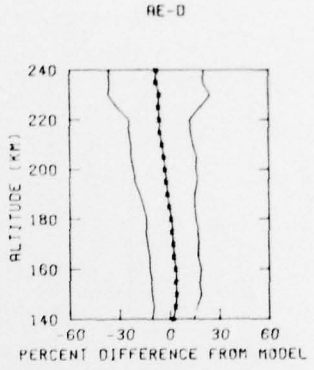

Figure 14b. Percent Deviation from the MSIS Model of the Mean and Standard Deviations of AE-D Density Measurements vs Altitude

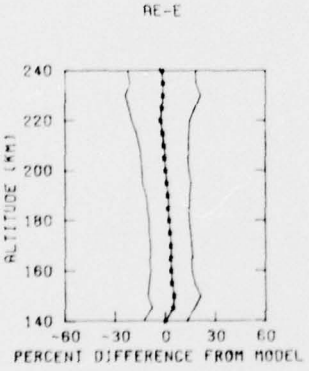

Figure 14c. Percent Deviation from the MSIS Model of the Mean and Standard Deviations of AE-E Density Measurements vs Altitude

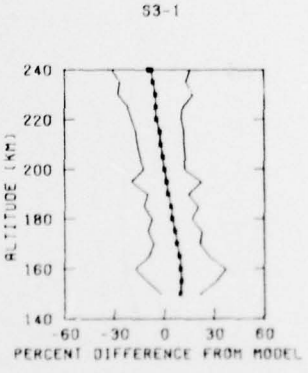

Figure 14d. Percent Deviation from the MSIS Model of the Mean and Standard Deviations of S3-1 Density Measurements vs Altitude

3.5 Local Time Variations

A description of the daily variations in the lower thermospheric density was obtained using AE-E data. This satellite was used because of its low inclination and excellent local time coverage. Data at 160, 200, and 240 km were separated into 1-hr local time bins and averaged. Similarly an average ratio to J71 and to MSIS was calculated for each bin. The results at these three heights are plotted in Figure 15. Average density values are shown as solid lines, crosses represent ratios to J71, and circles represent ratios to MSIS. Figure 15 (160 km) shows a density minimum, rather than maximum, near 1400 hours. Two nearly equal maxima are observed, one near 0700 and one near 2100 hours. Evidence of the diurnal bulge is seen, increasing with altitude at 200 and 240 km. These results are characteristic of atmospheric tidal variations.[13] The J71 model does not include local time variations due to tides. The density is underestimated from early evening hours to late morning hours. Ratios vary by about 30% for the data shown in Figure 15. MSIS does include tidal components. The observed variations are more closely represented and the agreement is within +9 to -1%. Figures 16a and 16b show an example of the frequency distributions for a specific local time interval. Data obtained at all altitudes in the 0800-0900 bin are shown. Relative to J71, $\bar{x}$ is 11.2% and S is 11.9%. For MSIS these values are 5.39% and 11.92%, respectively.

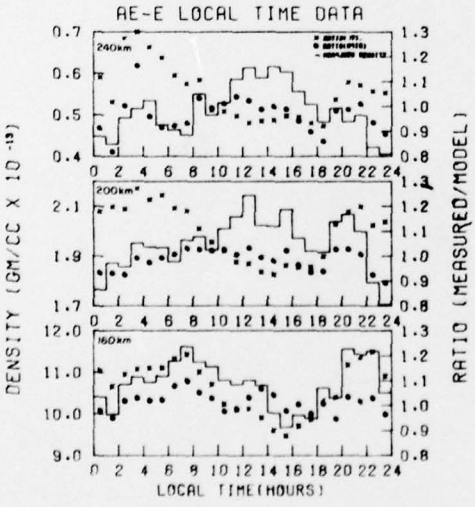

Figure 15. Local Time Variation of AE-E Density Data at 160, 200, and 240 km; Ratio of Data to J71 and MSIS

13. Mayr, H.G., Harris, I., and Volland, M. (1973) Theory of the phase anomaly in the thermosphere, J. Geophys. Res. 78:7480.

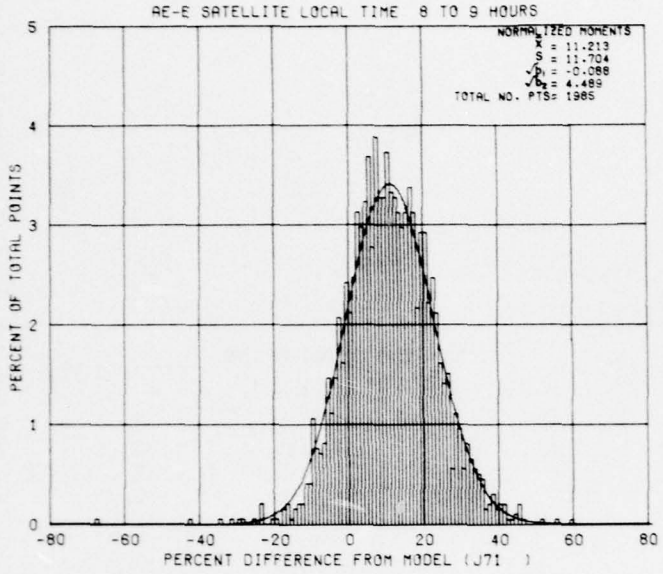

Figure 16a. Frequency Distribution of Percent Difference of AE-E 0800-0900 Data from J71 Model

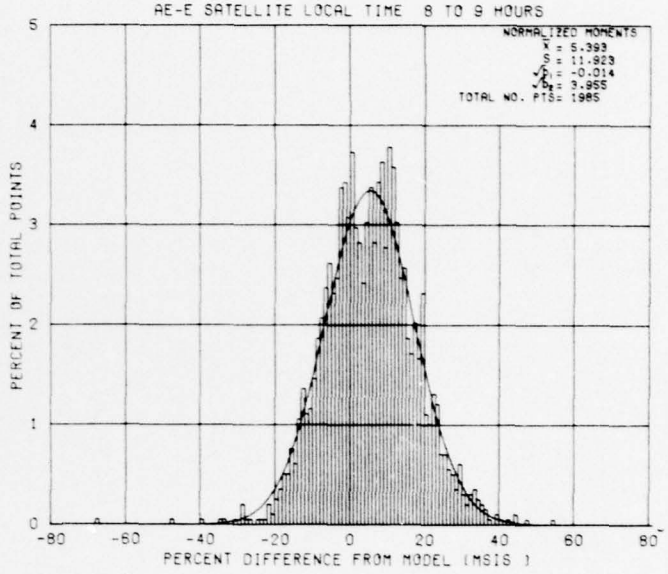

Figure 16b. Frequency Distribution of Percent Difference of AE-E 0800-0900 Data from MSIS Model

The AE-E data are further examined in Figure 17 which shows the density values at 5 km intervals from 145-240 km as a function of local time. To permit better analysis of the relative tidal amplitudes the data have been normalized to an altitude of 180 km. Newton et al[14] have detected tidal variations in the altitude region 220 - 280 with the San Marco satellite (inclination 3°). Between 220 and 25 km, where comparison can be made, their results agree in general with those of Figure 16. However, the semi-diurnal component appears to be less pronounced in their data. The difference may be attributable to different solar and geophysical conditions for AE-E and San Marco. The AE-E data cover a wider latitudinal and seasonal range and were obtained during lower solar flux conditions than that of Newton et al. A report describing the amplitude and phase of the observed AE-E local time variations is in preparation.

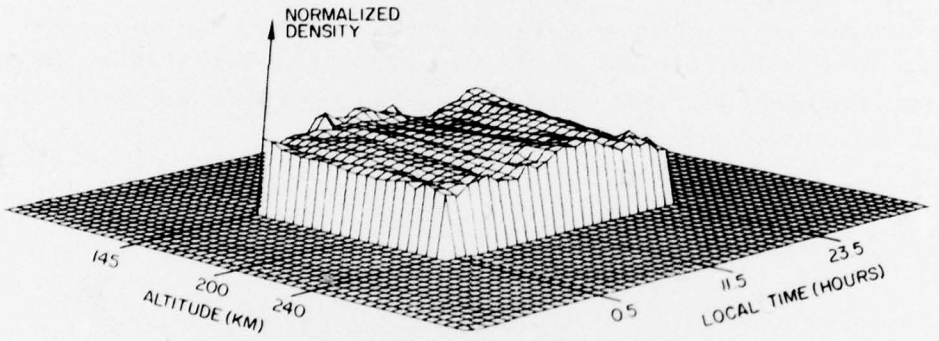

Figure 17. Altitude Dependence of AE-E Local Time Variations (Normalized to 180 km)

4. CONCLUSIONS

An extensive data base has been developed utilizing accelerometer measurements obtained with four low altitude satellites. In addition to density values the data base incorporates appropriate satellite orbital information, solar and geophysical parameters and atmospheric model values. A description of the satellites, the accelerometer experiment, and the data has been given. It is anticipated that this data base will be useful for correlative studies of aeronomical problems requiring knowledge of the neutral atmosphere. The present study has been directed toward a statistical analysis of atmospheric variability. Several methods of displaying the data were developed. Analyses included determination of mean values

14. Newton, G.P., Kasprzak, W.T., Curtis, S.A., and Pelz, D.T. (1975) Local time variation of equatorial thermospheric composition determined by the San Marco 3 Nace, J. Geophys. Res. 80:2289.

and the second, third, and fourth moments about the mean. Comparison has been made with two commonly used atmospheric models, J71 and MSIS. Results have been presented in Figures 8 through 17 and Table 2. These data give the extent of unmodeled variations as a function of geomagnetic activity, latitude, altitude, and local time. Neither model gives a completely adequate description of the observed atmospheric variability as a function of all these parameters. The J71 model gives a better representation of the average geomagnetic activity effect. MSIS more accurately describes the near equatorial, low geomagnetic activity conditions. Because of systematic errors, due mainly to drag coefficient uncertainties, it cannot be determined whether the absolute value of density is more accurately represented by J71 or MSIS. Model deficiencies are observed in the depiction of local time variations, particularly near 160 km although MSIS provides a better depiction than J71. An evaluation of other models including the revised J71 model[15] is planned. The data base will be utilized to develop an improved model of the lower thermosphere extending the results of Marcos et al[16] which used only AE-C data. It is anticipated that this model will describe the density data in this report as a function of latitude, longitude, altitude, geomagnetic activity, and local time.

---

15. Jacchia, L. G. (1977) Thermospheric Temperature, Density and Composition: New Models, Spec. Rept. 375, Smithsonian Astrophys. Observatory, Cambridge, MA.

16. Marcos, F. A., Garrett, H. B., Champion, K. S. W., and Forbes, J. M. (1977) Density variations in the lower thermosphere from analysis of the AE-C accelerometer measurements. Planet. Space Sci. 25:499.

References

1. Devries, L. L. (1971) Experimental Evidence in Support of Joule Heating Associated With Geomagnetic Activity, Marshall Space Flight Center, NASA TM X-64568.

2. Marcos, F. A., McInerney, R., Corbin, J., Fioretti, R., and Grossbard, N. (1972) Atmospheric Density Results Derived From the SPADES Satellite Accelerometer Data, AFCRL-72-0608.

3. Jacchia, L. G. (1971) Revised Static Models of the Thermosphere and Exosphere With Empirical Temperature Profiles. Spec. Rept. 332, Smithsonian Astrophys. Observatory, Cambridge, MA

4. Hedin, A. E., Salah, J. E., Evans, J. V., Reber, C. A., Newton, G. P., Spencer, N. W., Kayser, D. C., Alcayde, D., Bauer, P., Cogger, L., and McClure, J. P. (1977a) A global thermospheric model based on mass spectrometer and incoherent scatter data, MSIS 1, N_2 density and temperature. J. Geophys. Res. 82:2139.

5. Hedin, A. E., Reber, C. A., Newton, G. P., Spencer, N. W., Brinton, H. C., and Mayr, H. G. (1977b) A global thermospheric model based on mass spectrometer and incoherent scatter data, MSIS 2. Composition, J. Geophys. Res. 82:2148.

6. Dalgarno, A., Hanson, W. B., Spencer, N. W., and Schmerling, E. R. (1973) The Atmosphere Explorer mission, Radio Sci. 8:263.

7. Champion, K. S. W., and Marcos, F. A. (1973) The triaxial accelerometer system on Atmosphere Explorer, Radio Sci. 8:197.

8. Noonan, J. P., Fioretti, R. W., and Hass, B. (1975) Digital Filtering Analysis Applied to the Atmosphere Explorer-C Satellite MESA Accelerometer Data, AFCRL-TR-75-0293.

9. Cage, A. L., and Zawalick, E. J. (1972) A Discussion of the Geomagnetic Indices K_p and A_p, 1932 to 1971, AFCRL-72-0693.

10. Snedecor, G. W., and Cochran, W. G. (1967) Statistical Methods, Iowa State University Press, Iowa

11. Marcos, F.A., and Champion, K.S.W. (1972) Variations of the neutral atmospheric density at low satellite altitudes, Proc. International Conf. on Aerospace and Aeronautical Meteorology, Washington, D.C.

12. Karr, G.A., and Smith, R.E. (1972) Influence of satellite aerodynamics on atmospheric density determination, Proc. International Conf. on Aerospace and Aeronautical Meteorology, Washington, D.C.

13. Mayr, H.G., Harris, I., and Volland, M. (1973) Theory of the phase anomaly in the thermosphere, J. Geophys. Res. 78:7480.

14. Newton, G.P., Kasprzak, W.T., Curtis, S.A., and Pelz, D.T. (1975) Local time variation of equatorial thermospheric composition determined by the San Marco 3 Nace, J. Geophys. Res. 80:2289.

15. Jacchia, L.G. (1977) Thermospheric Temperature, Density and Composition: New Models, Spec. Rept. 375, Smithsonian Astrophys. Observatory, Cambridge, MA.

16. Marcos, F.A., Garrett, H.B., Champion, K.S.W., and Forbes, J.M. (1977) Density variations in the lower thermosphere from analysis of the AE-C accelerometer measurements. Planet. Space Sci. 25:499.